Accepted Manuscript

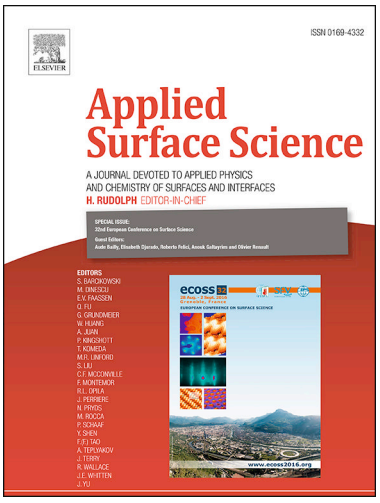

Full Length Article

Interfacial bonding mechanisms between aluminum and titanium during cold gas spraying followed by friction-stir modification

F. Khodabakhshi, B. Marzbanrad, H. Jahed, A.P. Gerlich

PII: S0169-4332(18)32292-X
DOI: https://doi.org/10.1016/j.apsusc.2018.08.156
Reference: APSUSC 40193

To appear in: *Applied Surface Science*

Received Date: 20 May 2018
Revised Date: 3 August 2018
Accepted Date: 18 August 2018

Please cite this article as: F. Khodabakhshi, B. Marzbanrad, H. Jahed, A.P. Gerlich, Interfacial bonding mechanisms between aluminum and titanium during cold gas spraying followed by friction-stir modification, *Applied Surface Science* (2018), doi: https://doi.org/10.1016/j.apsusc.2018.08.156

Interfacial bonding mechanisms between aluminum and titanium during cold gas spraying followed by friction-stir modification

F. Khodabakhshi[a*], B. Marzbanrad[b], H. Jahed[b], A.P. Gerlich[b]

[a] School of Metallurgical and Materials Engineering, College of Engineering, University of Tehran, P.O. Box: 11155-4563, Tehran, Iran

[b] Department of Mechanical and Mechatronics Engineering, University of Waterloo, Waterloo, ON, Canada

[*]Corresponding author: Tel: +98 (21) 8208 4127, Fax: +98 (21) 8800 6076; E-mail: fkhodabakhshi@ut.ac.ir, farzadkhodabakhshi83@gmail.com (F. Khodabakhshi)

Abstract

This paper closely evaluates the interfacial bonding mechanism between titanium particles deposited on an aluminum alloy substrate by cold gas spraying followed by friction-stir processing (FSP). After cold spraying and FSP modification, the produced Al/Ti interface was studied using focus ion beam-transmission electron microscopy (FIB-TEM) analysis and auger electron spectroscopy. Formation of a well-bonded titanium aluminide reaction layer was observed at the interface with a thickness in the range of 10-20 nm and a coherent interface associated with an inter-diffusion distance of about 600 nm. The results of this study showed that the physical bonding phenomenon during cold spraying according to the well-known adiabatic shear instability at the interface can be associated with chemical bonding and formation of an intermetallic layer at the interface during FSP modification. This is aided by the induced thermo-mechanical processing and deformation-assisted solid-state diffusion-based reactions. Also, these possible interfacial bonding and intermetallic layer formation mechanisms were discussed based on the inter-diffusion of elements at the Al/Ti interface based on the well-established Boltzmann-Matano theory and kinetics models correlated with experimental observations. The main findings of this research highlight the role of FSP on the performance of cold spray coatings as a post-processing technique to promote densification and homogenization during processing by promoting nano-scale interfacial mechanisms and chemical bonding at the interface.

***Keywords**:* Aluminum substrate; Ti-coating; Cold spray; Friction-stir processing; Bonding mechanism; Modeling

1. Introduction

Cold gas dynamic spraying is a new and versatile solid-state coating technology which can be easily implemented in the field. It utilizes the high velocity kinetically impact of particles upon the substrate to achieve bonding without melting. It only relies on severe plastic shear deformation to achieve deposition of the powder materials with minimum possible oxidation, structural/compositional changes, and undesirable phase transformations when compared to conventional high temperature thermal spraying technology [1, 2]. Beneficial residual stress induced by the peening process [3] and potentials for fatigue life enhancement of substrate [4] have added to the attractions of cold spray coating. Also, this technology can be implemented to repair the damaged structures and for rapid/additive layer by layer manufacturing with higher deposition rates as compared to the selective laser/electron-beam melting based methods [5-7].

During the build-up of material by cold spraying, the adhesion of coated material is influenced by the cohesion and adhesion strengths mainly due to “particle to particle compaction” between the layers as well as the “particle to substrate interaction” in the first layer, respectively [8, 9]. Highly pressurized nitrogen or helium inert? gas streams in the range of 1.5 MPa are usually employed to fluidize and transfer the typically micro-sized particles on the substrate surface and accelerate them through a convergent-divergent type nozzle with a high velocity impact in the range of 500-1200 m/sec to produce strain rates in the order of 0.5×10^{9}/s for nanosecond durations on impact, depending on the type of substrate, particles, carrier gas, flow gas temperature and nozzle design [10, 11].

This new technology has attracted considerable attention in the academia for about ten years, which has spurred new industrial applications aside from thermal spraying methods, considering the unique performance of the coatings as well as the economic efficiency [12].

Improvement of surface characteristics including indentation hardness, wear resistance, fatigue fracture, corrosion, electrical resistivity, and thermal conductivity were the main objects of cold spray depositions [13, 14]. The first application of cold gas spraying technology has involved manufacturing of dense and strongly bonded oxygen-free copper coatings with superior physical and mechanical properties [15]. Thereafter, it was extended to other materials sensitive to oxidation and heat, such as titanium, magnesium, metastable and nanocrystalline materials [16, 17].

Since the integrity and performance of cold sprayed coatings can be controlled by the bonding quality between particles and substrate during high velocity impact process, understanding the nature of bonding mechanism is essential to explore new coating applications [18]. Mechanisms used to explain bonding during explosive welding [19] or shock wave powder compaction [20] processes are very similar to those involved during cold gas spraying, in terms of formation of material flow jet upon impact, subsequent widespread severe plastic deformation, and the related phase transformation phenomena at the interface. The required heat and material flow controlling interfacial bonding are generated by adiabatic shear instability and subsequent thermal softening [18, 21]. Adiabatic shear instability is a well-known micro-mechanism which has been introduced by Assadi et al. [22], and is a dominant feature of bonding during particle impact in cold spraying. This heating is induced by the high strain rate severe plastic deformation at the interface without any melting in a time period of less than 100 ns. Physical bonding involving this mechanism is achieved using gas flow rates higher than a critical impact velocity which depend on the gas pressure and temperature, as well as the powder and substrate thermo-mechanical characteristics, which all depend on the temperature, strain, and strain-rate fields produced during particle impingement on the surface [23, 24].

Friction-stir processing (FSP) is an innovative and energy efficient adaption of

friction-stir welding (FSW), which was introduced by Mishra et al. [25, 26] mainly for the aim of localized surface microstructural modifications in metallic materials. In this solid-state processing technique, a non-consumable and specially designed rotating tool is forged on the surface of substrate, leading to localized frictional heating mainly due to the contact between shoulder and substrate. This causes the material to soften under the shoulder surface and around the pin as a result of induced severe plastic shear straining, and by traversing the tool along the pre-defined path, material is transferred from the leading edge to trailing, such that upon cooling a modified stirred zone is produced with a refined microstructure [27].

This modification technique has been employed for the purpose achieving desirable material properties, including; (*i*) fabrication of ultra-fine grained metals to attain high strain rate superplasticity [28, 29], (*ii*) production of metal-matrix nanocomposites [30-33], (*iii*) homogenizing of powder metallurgy products [34-36], and (*iv*) eliminating the casting defects [27]. More recently, FSP was implemented as an effective post-processing technique to consolidate pores and remove the micro-cracks, enhance the uniformity, refine the microstructure, and subsequently improve the mechanical performance of cold sprayed coatings [37-45]. One possible and important effect of the FSP modification step can be its action as a thermo-mechanical treatment to improve the cohesive bonding strength of a cold sprayed interface by activating solid-state diffusion phenomena which can avoid possible detrimental grain coarsening during post annealing heat-treatment [38, 39]. However, the influence of friction-stir modification on the bonding mechanism and strength at the interface of the cold sprayed coating layer was not studied yet or addressed well.

Therefore, the present research focused on the effects of post friction-stir processing to reveal the interfacial bonding mechanisms at the interface between cold-sprayed aluminum and titanium by using auger electron spectroscopy and transmission electron microscopy (TEM) analyses. Also, the possible phase transformations and interfacial phenomena at the

interaction region were studied based on well-established diffusion kinetics theories.

2. Experimental procedure

A plate of AA5083-H34 aluminum alloy with a thickness of 10 mm and standard chemical composition as reported in Table 1 was used as the substrate. The sample surface was finely grinded and cleaned before cold spray coating. Pure titanium powder with a spherical morphology and a particle size in the range of 20-80 μm, as shown in Fig. 1, was supplied from the TLS Company (TLS, Germany) to utilize for coating. The coating was performed using an SST-P low-pressure cold spray machine equipped with a powder feeder (4000 series, 5MPE, USA) made by Centerline Company (Windsor, Canada). Nitrogen was used as the carrier gas through a convergent-divergent DeLaval nozzle with a length of 120 mm and an orifice diameter of 2 mm for transferring the titanium particles from powder feeder on the surface of substrate. By optimizing the main cold spray processing parameters as gas pressure of 1.4 MPa (203 psi), gas temperature of 500 ºC, powder feeding rate of 2.24 gr/min, stand-off distance of 12 mm, gun traverse speed of 2.5 mm/sec and hatching distance of 2.5 mm. A titanium coating layer with the thickness of around 800 μm was successfully deposited on the surface of aluminum substrate. After sectioning across the thickness, standard metallographic sample preparation was performed similar to the details in the refs [30, 46, 47].

A porous cold spray coating layer with about 70% densification is shown in optical macrographs of Fig. 2. Friction-stir processing (FSP) was considered to modify and consolidate the cold spray coating to improve its integrity. For this purpose, a Jafo manual milling machine was implemented by using a pin-less cylindrical tool with a shoulder diameter of 12 mm. To avoid the undesirable solid-state chemical reactions between FSP tool and titanium coating layer during process, a tungsten carbide tool was used. The processing

parameters used for FSP modification involved a tool rotational speed (*w*) of 900 rpm, traverse velocity (*v*) of 63 mm/min, with a constant plunge depth and nuting-angle of about 0.5 mm and 2.5°, respectively. The effects of FSP modification step on the cold spray deposited titanium coating layer are shown in macro-images of Fig. 2, as well. In the composite field emission-scanning electron microscopy (FE-SEM) macro-images of Fig. 3, significant densification of the porous cold spray coating layer can be noted after this FSP step.

The main objective of the present research is studying the interface between titanium coating layer and aluminum substrate after cold spray deposition and after FSP modification. A Zeiss Leo 1530 FE-SEM microscope (ZEISS, Germany) operated at an accelerated voltage of ~30 keV was used for imaging and chemical analysis. A thin foil sample was prepared from the interface by a ZEISS Crossbeam 540 focused ion beam-scanning electron microscope (FIB-SEM, ZEISS, Germany) and thereafter analyzed under two JEOL 2010F (JEOL, Japan) and FEI Titan LB (FEI, USA) microscopes with capabilities for high contrast and high resolution imaging, energy-dispersive X-ray spectroscopy (EDS), and electron energy loss spectroscopy (EELS) analysis. The Image-J software was employed for crystallographic diffraction analysis of the atomic orientations based on Fast Fourier Transform (FFT) algorithm. Furthermore, to monitor the chemical composition changes at the interaction layer auger electron spectroscopy (AES) analysis was performed by using a JAMP 9500F auger microprobe (JEOL-9500F, Japan) with a detection limit of up to ~5 nm combined on the ZEISS FE-SEM microscope. A line-scan analysis with distance intervals of about 100 nm was carried out across the Al/Ti interface. Mechanical property of the modified cold spray coating after FSP from different locations of coating layer as compared to the interface and base metals was elaborated in terms of micro-hardness mapping. A Buehler micro-indenter machine (Buehler, Germany) was used with a Vickers indenter and load of

300 gr for a 15 sec dwell time.

3. Results and discussion

3.1 Transmission electron microscopy characterization

Figures 4a-c and 4d-f show the FE-SEM images from the Al/Ti interface after cold spraying and FSP respectively. The locations for extracting the thin-foil samples are indicated in the same figures. Different ion milling/polishing steps to prepare the thin foil (<100 nm) for TEM analysis from the Al/Ti interface are presented in FE-SEM images of Fig. 5. In Fig. 6, bright-field TEM images obtained using a JEOL microscope from the interface between aluminum substrate and titanium coating layer, with an embedded Ti-particle at the substrate are shown. The wavy morphology of interface can be attributed to the explosive-like strain field at the interface as induced by particles impingement during cold spraying process [48, 49]. The EDS elemental mapping results by TEM analysis of the Al/Ti interface from two regions are presented in Fig. 7. High magnification TEM images from the sub-grain structure of titanium close to interface in Fig. 8 indicates the formation of a cellular structure with an average size less than 200 nm caused by the severe plastic deformation of impact process in which, there is a short time for activating the static or dynamic restoration mechanisms. Figure 9 show a TEM image from the selected location of Al/Ti interface for further studies with more details within the interaction layer at high magnifications under the JEOL and Titan LB microscopes. In high resolution TEM images shown in Fig. 10, formation of a very thin layer from a different phase is observable. High magnification HRTEM images from the Al/Ti interface provide strong contrast between the aluminum and titanium alloy regions are shown in Fig. 11. The presence of a thin interaction layer with different contrast at the interface is clearly evident.

Some complex precipitates within the aluminum matrix are visible close to the

interface in Fig. 9, as well. Complex Al-Fe-Mn-Si precipitates with semi-spherical morphologies within the aluminum alloy matrix are shown with strong Z-contrast are revealed by high angle annular dark field (HAADF) TEM in Fig. 11d. To study the crystal structure and chemical composition of this interaction layer at the interface, further examinations were followed by high resolution imaging, crystallographic orientation, and elemental chemical analysis using the Titan LB TEM microscope. High resolution TEM images from this interaction layer between aluminum and titanium at the interface are illustrated in Fig. 12. The thickness of the layer varies in the range of 10-20 nm. The variation may be associated with the induced temperature and strain fields during cold gas spraying process. However, an average thickness size of around 10 nm can be estimated for this interaction layer. In high magnification HRTEM images in Fig. 13, the orientation of atoms at the interface with respect to substrate and coating layer can be evaluated. In atomic orientations, some wavy shape flow paths can be seen which can be attributed to the severe shear straining action of rotating tool during FSP [50, 51].

The FFT analysis results and crystallographic orientations are discussed and presented in combination with an HR-TEM image from the interaction layer in Fig. 14. Based on the FFT analysis and the related diffraction spot patterns from the interface, the new phase at the interaction layer appears to correspond to a titanium aluminide compound showing a $D0_{22}$ tetragonal crystal structure with a *d*-spacing of ~2.29 A° in accordance with the lattice constants of Al_3Ti phase [33, 52, 53]. This interaction layer exhibits a great atomistic matching with the both aluminum substrate and titanium coating layer by showing two crystallographic orientation relationships as $\left(\bar{1}\,\bar{1}2\right)_{Al_3Ti} \perp \left(111\right)_{Al}$ and $\left(\bar{1}\,\bar{1}2\right)_{Al_3Ti} \perp \left(\bar{1}01\right)_{Ti}$, respectively (see Fig. 14). Moreover, the EELS elemental mapping chemical analysis results from the interaction layer at high magnifications as demonstrated in Fig. 15 are in a good agreement with the apparent Ti-Al phase identification. The extend of reaction layer at the

interface is traceable based on the oxygen map of EELS analysis showing some build-up of O element at a layer with a thickness in the range of 10-20 nm. However, since there is only a slight difference between the level of oxygen in the titanium matrix and interface, it seems that the oxygen was only diffused as impurity in the structure of intermetallic layer at the interface, and there is a low probability for formation of a compound structure which includes oxygen.

Formation of this thermodynamically-stable titanium aluminide phase at the interaction layer which produced a well-bonded interface between the aluminum substrate and titanium coating layer after cold spraying and subsequent FSP modification is a result of involved thermo-mechanical phenomena [37, 54]. Therefore, this "interaction layer" actually can be considered as a "reaction layer" by formation of a new chemical compound at the interface based on the inter-diffusion of elements during thermo-mechanical process. The interfacial bonding mechanisms between substrate and coating layer for the studied system can be proposed to involve "chemical bonding" by formation of the mentioned intermetallic layer at the interface. This is complimentary to "physical bonding" according to the well-established adiabatic shear instability at the interface as introduced by Assadi et al. [22] for bonding between the metallic particles and substrate during cold spraying process [55-58]. It seems that FSP also has beneficial influence on the kinetics for development of intermetallic layer at the interface due to thermo-mechanical post-treatment action and accordingly the related solid-state chemical reactions aided by intense plastic deformation during process.

3.2 Auger electron spectroscopy analysis from the Al/Ti interface

Auger electron spectroscopy is a highly surface-sensitive quantitative elemental and chemical-state analysis technique to attain the compositional information from the sample allowing one to characterize the nanoscale features by exciting auger electrons and quantifying the energy and intensity of emitted electrons with a typical interaction depth of

less than 5 nm [59]. Fig. 16a,b presents results of characterization of the interaction layer by this surface analysis technique. The gradual variation in the chemical composition of aluminum and titanium elements across the interface is clearly seen in this figure. The presence of an inter-diffusion layer with the thickness of ~600 nm at the interface, which can be attributed to inter-diffusion of aluminum and titanium elements across the interface, based on these auger spectroscopy analysis results is evident (see Fig. 16c). A sharp transition of elements across the interface indicates the low thickness of intermetallic layer at the interaction region which agrees well with the direct HR-TEM observations shown in Fig. 13. Also, this concentration gradient profile was used for diffusion modeling to predict the inter-diffusion coefficient and the thickness of reaction layer as will be explained in what follows.

3.3 Diffusion modeling

3.3.1 Inter-diffusion coefficient and Boltzmann-Matano theory

Although the interaction time during particle impact is <100 ns in cold spray which may be not enough for diffusion, there is evidence that a limited diffusion occurred at the interface because of the high temperature imposed during subsequent FSP treatment. The Al_3Ti intermetallic layer at the interface can be formed mainly by diffusion of aluminum through titanium in the Al-Ti diffusion couple [60, 61]. The Boltzmann-Matano diffusion theory [62] can be employed for modeling the diffusion phenomenon in concentrated alloys as induced by chemical composition gradient. In our case, the inter-diffusion coefficient is indicated by parameter $\tilde{D}$ in the non-steady-state one dimensional Fick's second law diffusion equation [63]:

$$\frac{\partial C}{\partial t} = \left(\frac{\partial}{\partial x}\right)\left(\tilde{D}\frac{\partial C}{\partial x}\right) \tag{1}$$

where C is the concentration of tracer element as a function of position (x) and time (t). By

substituting a new variable as $\eta = \frac{x}{\sqrt{t}}$ (also known as Boltzmann parameter) in the above relation, the partial differential equation is transformed to a simple ordinary differential equation [63].

$$\frac{-\eta}{2}\frac{dC}{d\eta} = \frac{d}{d\eta}\left(\tilde{D}\frac{dC}{d\eta}\right) \tag{2}$$

The inter-diffusion coefficient can be derived after application of boundary condition ($C = 0$ for $\eta = -\infty$, and $C = C_0$ for $\eta = +\infty$) [63]:

$$\tilde{D}(C) = -\left(\frac{1}{2t}\right)\left(\frac{dx}{dC}\right)\int_0^C x dC' \tag{3}$$

where $\int x dC = 0$ is the Matano-plane [63]. Darken [63] introduced the inter-diffusion phenomenon based on the actual driving force as chemical free-energy gradient:

$$\tilde{D}(C) = X_A D_A + X_B D_B \tag{4}$$

$$D = D_0 \exp\left(-\frac{Q}{RT}\right) \tag{5}$$

where X is the atomic fraction of elements, D_0 is the pre-exponential factor depending on temperature, Q is the activation energy for diffusion, R is the gas universal constant (~8.314 J.mole^{-1}.K^{-1}), and T is the processing temperature [63].

The auger electron spectroscopy chemical analysis along the scan-line across interface in Fig. 16a as results shown in Fig. 16b with a high spatial resolution was considered as input of concentration gradient for both theories to predict the inter-diffusion coefficient. Temperature of stirred zone inside the pure titanium during FSP was taken as 950 °C for the employed processing parameters [64, 65], which is higher than the α to β phase

transformation temperature (~882 °C) for pure titanium [66]. Therefore, high temperature severe plastic deformation of pure titanium during FSP was accomplished under the β-phase crystal structure. In this research, the temperature on the surface of titanium coating under the shoulder action maybe can reach to the such high values, but temperature at the interface that accelerate the inter-diffusion of elements across the interface would be certainly lower than the melting of aluminum. Pre-exponential factors for diffusion of aluminum (considering its concentration in the examined AA5083 aluminum alloy of ~93%) through the β-phase pure titanium and vice versa at this range of assessment for temperature of SZ were considered as $D^0_{Al} = 5.31\times10^{-6} m^2.s^{-1}$ and $D^0_{Ti} = 3.03\times10^{-4} m^2.s^{-1}$, respectively [53, 61, 67, 68]. Also, the activation energies for these diffusion phenomena were estimated in the literature as $Q^D_{Al} = 220.8 kJ.mole^{-1}$ and $Q^D_{Ti} = 325 kJ.mole^{-1}$, respectively [61, 67, 68]. Since the heating during FSP process is mostly attributed to the frictional flow of materials on the surface and induced by the rotating shoulder of tool [25, 69], by considering the shoulder diameter of 12 mm and tool traverse velocity of 63 mm/min, the holding time for each point at peak temperature of FSP can be estimated around 11.4 sec. In Fig. 16c, the calculated inter-diffusion coefficient ($\tilde{D}$) is plotted as a function of position (composition) according to the both of Boltzmann-Matano and Darken's theories. Based on the plot, and by equating left and right areas, the X_m, which described the Boltzmann-Matano interface, is determined to be ~1.35 μm. As expected, the maximum inter-diffusion coefficient is measured at about 8.6×10^{-14} $m^2.sec^{-1}$ with a very sharp peak at the interface. This value was utilized in the kinetics model for prediction of intermetallic layer formation and growth at the Al/Ti interface during subsequent friction-stir modification as will be explained in what follows.

3.3.2 Kinetics of intermetallic layer formation and growth at the interface

Formation of intermetallic compounds between the dissimilar metals in thermally-

activated processes is a common phenomenon due to diffusion bonding by inter-diffusion of different atoms across the interface [33, 61, 70, 71]. The growth of the reactive layer at the interface is controlled by high temperature bulk/volume diffusion and its kinetics can be described by a relation between temperature and time of annealing in an Arrhenius equation [70]:

$$x^2 = \alpha\sqrt{K\tilde{D}^n t} \tag{6}$$

$$K = K_0.\exp\left(-\frac{Q}{RT}\right) \tag{7}$$

$$x^2 = \alpha t\sqrt{K_0 \exp\left(-\frac{Q}{RT}\right)\tilde{D}^n} \tag{8}$$

where x is the thickness of the reactive layer at the interface, α is a proportionality constant (~4), K is the parabolic coefficient, $\tilde{D}$ is the inter-diffusion coefficient at the interface (~8.6×10^{-14} $m^2.sec^{-1}$), n is the diffusion exponent (~2.2), t is the holding time at processing temperature during FSP (~11.4 sec), K_0 is the temperature-independent pre-exponential factor (~6700 $m^2.sec^{-1}$), Q is the activation energy for diffusion of aluminum through titanium (~220.8 $kJ.mole^{-1}$), R is the gas universal constant (~8.314 $J.mole^{-1}.K^{-1}$), and T is the temperature at the interface (<933 K, *i.e.*, melting temperature of aluminum) during FSP without pin on the surface of pure titanium [61, 70]. By substituting these equivalent values for the case of present study in the above equation, the thickness of intermetallic layer at the interface due to reactive chemical bonding is found to be 17.5 nm, which is consistent with the experimental results of direct HR-TEM observations from the Al/Ti interface in the range of 10-20 nm (see Figs. 10 to 14).

3.4 Indentation hardness

Figure 17 illustrate the indentation Vickers micro-hardness maps from the aluminum

substrate, toward the interface and titanium coating layer. As seen, the aluminum substrate has a hardness value of ~95 HV. By cold spray coating and thereafter friction-stir modification, the hardness of Ti-coating layer is considerably increased mainly due to (*i*) densification, (*ii*) grain refinement, (*iii*) chemical reactions, and (*iv*) martensitic phase transformation as induced by severe plastic deformation/stirring action of rotating tool and exposing against the atmosphere during process [37]. A maximum hardness number of up to ~630 HV is attained on the surface layer in contact with the tool shoulder. This extreme surface hardening corresponding to a 700% increase can be mainly due to the surface oxidation (TiO_2) and nitride formation (TiN) by absorption of O and N elements during process as well as the coating densification and grain size reduction induced by superior plastic material flow field of shoulder on the surface. As shown, by taking distance from the surface layer toward the interface with the aluminum substrate, the hardness value is gradually decreased down to values less than 200 HV. Also, it seems that the interaction layer did not show a noticeable effect on the micro-hardness profile. Titanium aluminide phase has a high hardness value in the range of 600-700 HV [33, 51], however, owing to its low thickness at the interface (~10 nm) cannot have a significant affect the indentation hardness.

4. Conclusions

The present research presents in-depth characterization of the interfacial bonding between titanium particles and aluminum substrate during cold gas spraying followed by friction-stir processing. Based on the findings, the adiabatic shear interlocking bonding mechanism between aluminum and titanium in cold spray is aided by a chemical bonding via deformation assisted solid-state chemical inter-diffusion of elements during FSP which leads to formation of a titanium aluminide (Al_3Ti) intermetallic reaction layer with a thickness of ~10-20 nm

within an inter-diffusion distance of ~600 nm. This new phase also exhibits excellent matching according to the $\left(\bar{1}\,\bar{1}2\right)_{Al_3Ti} \perp \left(111\right)_{Al}$ and $\left(\bar{1}\,\bar{1}2\right)_{Al_3Ti} \perp \left(\bar{1}01\right)_{Ti}$ crystallographic orientation relationships with the aluminum and titanium matrices, respectively. The presence of the inter-diffusion layer was backed up by inter-diffusion modeling of Al and Ti elements considering the real thermo-mechanical conditions for pure titanium during FSP modification. The Boltzmann-Matano and non-steady-state diffusion-based kinetic theories predicted the inter-diffusion coefficient ($\tilde{D}$) and the formation of an intermetallic layer at the interface in agreement with the experimental observations on the occurrence of chemical bonding during FSP.

Acknowledgements

Financial support from the Natural Sciences and Engineering Council of Canada is greatly appreciated.

References

[1] R. Maev, V. Leshchynsky, Impact Features of Gas Dynamic Spray Technology, Introduction to Low Pressure Gas Dynamic Spray, Wiley-VCH Verlag GmbH & Co. KGaA2008, pp. 11-35.

[2] V.K. Champagne, 1 - Introduction, The Cold Spray Materials Deposition Process, Woodhead Publishing 2007, pp. 1-7.

[3] B. Marzbanrad, H. Jahed, E. Toyserkani, On the evolution of substrate's residual stress during cold spray process: A parametric study, *Mater. Des.* 138 (2018) 90-102.

[4] S.B. Dayani, S.K. Shaha, R. Ghelichi, J.F. Wang, H. Jahed, The impact of AA7075 cold spray coating on the fatigue life of AZ31B cast alloy, *Surf. Coat. Technol.* 337 (2018) 150-158.

[5] S. Yin, B. Aldwell, R. Lupoi, Cold spray additive manufacture and component restoration, Cold-Spray Coatings: Recent Trends and Future perspectives 2017, pp. 195-224.

[6] R.N. Raoelison, C. Verdy, H. Liao, Cold gas dynamic spray additive manufacturing today: Deposit possibilities, technological solutions and viable applications, *Mater. Des.* 133 (2017) 266-287.

[7] Y.Q. Ren, P.C. King, Y.S. Yang, T.Q. Xiao, C. Chu, S. Gulizia, A.B. Murphy, Characterization of heat treatment-induced pore structure changes in cold-sprayed titanium, *Mater. Charact.* 132 (2017) 69-75.

[8] A. Moridi, S.M. Hassani-Gangaraj, M. Guagliano, M. Dao, Cold spray coating: Review of material systems and future perspectives, *Surf. Eng.* 30(6) (2014) 369-395.

[9] Z. Arabgol, M. Villa Vidaller, H. Assadi, F. Gärtner, T. Klassen, Influence of thermal properties and temperature of substrate on the quality of cold-sprayed deposits, *Acta Mater.* 127 (2017) 287-301.

[10] M. Grujicic, C.L. Zhao, C. Tong, W.S. DeRosset, D. Helfritch, Analysis of the impact

velocity of powder particles in the cold-gas dynamic-spray process, *Mater. Sci. Eng., A* 368(1-2) (2004) 222-230.

[11] T. Schmidt, H. Assadi, F. Gärtner, H. Richter, T. Stoltenhoff, H. Kreye, T. Klassen, From particle acceleration to impact and bonding in cold spraying, *J. Therm. Spray Technol.* 18(5-6) (2009) 794-808.

[12] V.K. Champagne, V.K. Champagne, C. Widener, Cold spray applications, Cold-Spray Coatings: Recent Trends and Future perspectives2017, pp. 25-56.

[13] Z. Arabgol, H. Assadi, T. Schmidt, F. Gärtner, T. Klassen, Analysis of thermal history and residual stress in cold-sprayed coatings, *J. Therm. Spray Technol.* 23(1-2) (2014) 84-90.

[14] H. Assadi, H. Kreye, F. Gärtner, T. Klassen, Cold spraying – A materials perspective, *Acta Mater.* 116 (2016) 382-407.

[15] S. Marx, A. Paul, A. Köhler, G. Hüttl, Cold spraying: Innovative layers for new applications, *J. Therm. Spray Technol.* 15(2) (2006) 177-183.

[16] A. List, F. Gärtner, T. Mori, M. Schulze, H. Assadi, S. Kuroda, T. Klassen, Cold Spraying of Amorphous $Cu_{50}Zr_{50}$ Alloys, *J. Therm. Spray Technol.* 24(1-2) (2014) 108-118.

[17] N. Cinca, J.M. Rebled, S. Estradé, F. Peiró, J. Fernández, J.M. Guilemany, Influence of the particle morphology on the Cold Gas Spray deposition behaviour of titanium on aluminum light alloys, *J. Alloys Compd.* 554 (2013) 89-96.

[18] M. Grujicic, J.R. Saylor, D.E. Beasley, W.S. DeRosset, D. Helfritch, Computational analysis of the interfacial bonding between feed-powder particles and the substrate in the cold-gas dynamic-spray process, *Appl. Surf. Sci.* 219(3-4) (2003) 211-227.

[19] M. Acarer, B. Gülenç, F. Findik, The influence of some factors on steel/steel bonding quality on there characteristics of explosive welding joints, *J. Mater. Sci.* 39(21) (2004) 6457-

6466.

[20] D. Yim, W. Kim, S. Praveen, M.J. Jang, J.W. Bae, J. Moon, E. Kim, S.J. Hong, H.S. Kim, Shock wave compaction and sintering of mechanically alloyed CoCrFeMnNi high-entropy alloy powders, *Mater. Sci. Eng., A* 708 (2017) 291-300.

[21] M. Grujicic, C.L. Zhao, W.S. DeRosset, D. Helfritch, Adiabatic shear instability based mechanism for particles/substrate bonding in the cold-gas dynamic-spray process, *Mater. Des.* 25(8) (2004) 681-688.

[22] H. Assadi, F. Gärtner, T. Stoltenhoff, H. Kreye, Bonding mechanism in cold gas spraying, *Acta Mater.* 51(15) (2003) 4379-4394.

[23] H. Assadi, T. Schmidt, H. Richter, J.O. Kliemann, K. Binder, F. Gärtner, T. Klassen, H. Kreye, On parameter selection in cold spraying, *J. Therm. Spray Technol.* 20(6) (2011) 1161-1176.

[24] T. Schmidt, F. Gärtner, H. Assadi, H. Kreye, Development of a generalized parameter window for cold spray deposition, *Acta Mater.* 54(3) (2006) 729-742.

[25] R.S. Mishra, Z.Y. Ma, Friction stir welding and processing, *Mater. Sci. Eng., R* 50(1–2) (2005) 1-78.

[26] R.S. Mishra, Z.Y. Ma, I. Charit, Friction stir processing: a novel technique for fabrication of surface composite, *Mater. Sci. Eng., A* 341(1–2) (2003) 307-310.

[27] Z.Y. Ma, Friction Stir Processing Technology: A Review, *Metall. Mater. Trans. A* 39(3) (2008) 642-658.

[28] R.S. Mishra, M.W. Mahoney, S.X. McFadden, N.A. Mara, A.K. Mukherjee, High strain rate superplasticity in a friction stir processed 7075 Al alloy, *Scr. Mater.* 42(2) (1999) 163-168.

[29] F. Khodabakhshi, A. Simchi, A.H. Kokabi, A.P. Gerlich, M. Nosko, Effects of stored strain

energy on restoration mechanisms and texture components in an aluminum–magnesium alloy prepared by friction stir processing, *Mater. Sci. Eng., A* 642 (2015) 204-214.

[30] F. Khodabakhshi, S. Arab, P. Švec, A. Gerlich, Fabrication of a new Al-Mg/graphene nanocomposite by multi-pass friction-stir processing: Dispersion, microstructure, stability, and strengthening, *Mater. Charact.* 132 (2017) 92-107.

[31] F. Khodabakhshi, A. Gerlich, P. Švec, Fabrication of a high strength ultra-fine grained Al-Mg-SiC nanocomposite by multi-step friction-stir processing, *Mater. Sci. Eng., A* 698 (2017) 313-325.

[32] F. Khodabakhshi, A. Gerlich, P. Švec, Reactive friction-stir processing of an Al-Mg alloy with introducing multi-walled carbon nano-tubes (MW-CNTs): Microstructural characteristics and mechanical properties, *Mater. Charact.* 131 (2017) 359-373.

[33] F. Khodabakhshi, A. Simchi, A.H. Kokabi, A.P. Gerlich, Friction stir processing of an aluminum-magnesium alloy with pre-placing elemental titanium powder: *In-situ* formation of an Al_3Ti-reinforced nanocomposite and materials characterization, *Mater. Charact.* 108 (2015) 102-114.

[34] F. Khodabakhshi, H. Ghasemi Yazdabadi, A.H. Kokabi, A. Simchi, Friction stir welding of a P/M Al–Al_2O_3 nanocomposite: Microstructure and mechanical properties, *Mater. Sci. Eng., A* 585 (2013) 222-232.

[35] F. Khodabakhshi, A. Simchi, A. Kokabi, A. Gerlich, M. Nosko, P. Švec, Influence of hard inclusions on microstructural characteristics and textural components during dissimilar friction-stir welding of an PM Al–Al_2O_3–SiC hybrid nanocomposite with AA1050 alloy, *Sci. Technol. Weld. Joining* 22(5) (2017) 412-427.

[36] F. Khodabakhshi, A. Simchi, A.H. Kokabi, A.P. Gerlich, Similar and dissimilar friction-stir

welding of an PM aluminum-matrix hybrid nanocomposite and commercial pure aluminum: Microstructure and mechanical properties, *Mater. Sci. Eng., A* 666 (2016) 225-237.

[37] F. Khodabakhshi, B. Marzbanrad, L. Shah, H. Jahed, A. Gerlich, Friction-stir processing of a cold sprayed AA7075 coating layer on the AZ31B substrate: Structural homogeneity, microstructures and hardness, *Surf. Coat. Technol.* 331 (2017) 116-128.

[38] T. Peat, A. Galloway, A. Toumpis, P. McNutt, N. Iqbal, The erosion performance of cold spray deposited metal matrix composite coatings with subsequent friction stir processing, *Appl. Surf. Sci.* 396 (2017) 1635-1648.

[39] T. Peat, A. Galloway, A. Toumpis, R. Steel, W. Zhu, N. Iqbal, Enhanced erosion performance of cold spray co-deposited AISI316 MMCs modified by friction stir processing, *Mater. Des.* 120 (2017) 22-35.

[40] M. Peel, A. Steuwer, M. Preuss, P.J. Withers, Microstructure, mechanical properties and residual stresses as a function of welding speed in aluminium AA5083 friction stir welds, *Acta Mater.* 51(16) (2003) 4791-4801.

[41] H. Ashrafizadeh, A. Lopera-Valle, A. McDonald, A. Gerlich, Effect of friction-stir processing on the wear rate of WC-based MMC coatings deposited by low-pressure cold gas dynamic spraying, Proceedings of the International Thermal Spray Conference, 2015, pp. 41-47.

[42] K.J. Hodder, H. Izadi, A.G. McDonald, A.P. Gerlich, Fabrication of aluminum–alumina metal matrix composites via cold gas dynamic spraying at low pressure followed by friction stir processing, *Mater. Sci. Eng., A* 556 (2012) 114-121.

[43] C. Huang, W. Li, Y. Feng, Y. Xie, M.P. Planche, H. Liao, G. Montavon, Microstructural evolution and mechanical properties enhancement of a cold-sprayed CuZn alloy coating with friction stir processing, *Mater. Charact.* 125 (2017) 76-82.

[44] C. Huang, W. Li, Z. Zhang, M. Fu, M.P. Planche, H. Liao, G. Montavon, Modification of a cold sprayed SiCp/Al5056 composite coating by friction stir processing, *Surf. Coat. Technol.* 296 (2016) 69-75.

[45] C. Huang, W. Li, Z. Zhang, M.P. Planche, H. Liao, G. Montavon, Effect of Tool Rotation Speed on Microstructure and Microhardness of Friction-Stir-Processed Cold-Sprayed SiCp/Al5056 Composite Coating, *J. Therm. Spray Technol.* 25(7) (2016) 1357-1364.

[46] F. Khodabakhshi, A.P. Gerlich, P. Švec, Reactive friction-stir processing of an Al-Mg alloy with introducing multi-walled carbon nano-tubes (MW-CNTs): Microstructural characteristics and mechanical properties, *Mater. Charact.* 131 (2017) 359-373.

[47] F. Khodabakhshi, A. Simchi, A. Kokabi, M. Nosko, P. Švec, Strain Rate Sensitivity, Work Hardening, and Fracture Behavior of an Al-Mg TiO_2 Nanocomposite Prepared by Friction Stir Processing, *Metall. Mater. Trans. A* 45(9) (2014) 4073-4088.

[48] H. Assadi, H. Kreye, F. Gärtner, T. Klassen, Cold spraying – A materials perspective, *Acta Mater.* 116(Supplement C) (2016) 382-407.

[49] H. Assadi, T. Schmidt, H. Richter, J.O. Kliemann, K. Binder, F. Gärtner, T. Klassen, H. Kreye, On Parameter Selection in Cold Spraying, *J. Therm. Spray Technol.* 20(6) (2011) 1161-1176.

[50] F. Khodabakhshi, M. Nosko, A.P. Gerlich, Effects of graphene nano-platelets (GNPs) on the microstructural characteristics and textural development of an Al-Mg alloy during friction-stir processing, *Surf. Coat. Technol.* 335 (2018) 288-305.

[51] F. Khodabakhshi, A. Simchi, A.H. Kokabi, P. Švec, F. Simančík, A.P. Gerlich, Effects of nanometric inclusions on the microstructural characteristics and strengthening of a friction-stir processed aluminum–magnesium alloy, *Mater. Sci. Eng., A* 642 (2015) 215-229.

[52] C.J. Hsu, C.Y. Chang, P.W. Kao, N.J. Ho, C.P. Chang, Al–Al_3Ti nanocomposites produced *in situ* by friction stir processing, *Acta Mater.* 54(19) (2006) 5241-5249.

[53] M. Thuillard, L.T. Tran, M.A. Nicolet, Al_3Ti formation by diffusion of aluminum through titanium, *Thin Solid Films* 166 (1988) 21-28.

[54] T.R. McNelley, S. Swaminathan, J.Q. Su, Recrystallization mechanisms during friction stir welding/processing of aluminum alloys, *Scr. Mater.* 58(5) (2008) 349-354.

[55] M. Grujicic, 9 - Particle/substrate interaction in the cold-spray bonding process A2 - Champagne, Victor K, The Cold Spray Materials Deposition Process, Woodhead Publishing 2007, pp. 148-177.

[56] M. Grujicic, J.R. Saylor, D.E. Beasley, W.S. DeRosset, D. Helfritch, Computational analysis of the interfacial bonding between feed-powder particles and the substrate in the cold-gas dynamic-spray process, *Appl. Surf. Sci.* 219(3–4) (2003) 211-227.

[57] M. Grujicic, C.L. Zhao, W.S. DeRosset, D. Helfritch, Adiabatic shear instability based mechanism for particles/substrate bonding in the cold-gas dynamic-spray process, *Mater. Des.* 25(8) (2004) 681-688.

[58] J. Henao, A. Concustell, S. Dosta, G. Bolelli, I.G. Cano, L. Lusvarghi, J.M. Guilemany, Deposition mechanisms of metallic glass particles by Cold Gas Spraying, *Acta Mater.* 125 (2017) 327-339.

[59] A.M. Ilyin, Chapter 11 - Auger Electron Spectroscopy A2 - Thomas, Sabu, in: R. Thomas, A.K. Zachariah, R.K. Mishra (Eds.), Microscopy Methods in Nanomaterials Characterization, Elsevier 2017, pp. 363-381.

[60] M. Thuillard, L.T. Tran, M.A. Nicolet, Al_3Ti formation by diffusion of aluminum through titanium, *Thin Solid Films* 166(C) (1988) 21-28.

[61] M. Mirjalili, M. Soltanieh, K. Matsuura, M. Ohno, On the kinetics of $TiAl_3$ intermetallic layer formation in the titanium and aluminum diffusion couple, *Intermetallics* 32 (2013) 297-302.

[62] B. Wierzba, W. Skibiński, The generalization of the Boltzmann–Matano method, *Physica A* 392(19) (2013) 4316-4324.

[63] A.K. Sinha, Physical Metallurgy Handbook, McGraw-Hill2003.

[64] B. Li, Y. Shen, L. Luo, W. Hu, Fabrication of TiCp/Ti–6Al–4V surface composite via friction stir processing (FSP): Process optimization, particle dispersion-refinement behavior and hardening mechanism, *Mater. Sci. Eng., A* 574 (2013) 75-85.

[65] B. Li, Y. Shen, W. Hu, L. Luo, Surface modification of Ti–6Al–4V alloy via friction-stir processing: Microstructure evolution and dry sliding wear performance, *Surf. Coat. Technol.* 239 (2014) 160-170.

[66] A. Shamsipur, S.F. Kashani-Bozorg, A. Zarei-Hanzaki, Production of *in-situ* hard Ti/TiN composite surface layers on CP-Ti using reactive friction stir processing under nitrogen environment, *Surf. Coat. Technol.* 218 (2013) 62-70.

[67] S.Y. Lee, O. Taguchi, Y. Iijima, Diffusion of aluminum in β-titanium, *Mater. Trans.* 51(10) (2010) 1809-1813.

[68] W.E. Alexander, J. Shackelford, CRC Materials Science and Engineering Handbook, Third Edition. , Boca Raton: CRC Press.2000.

[69] R. Nandan, T. DebRoy, H.K.D.H. Bhadeshia, Recent advances in friction-stir welding – Process, weldment structure and properties, *Prog. Mater Sci.* 53(6) (2008) 980-1023.

[70] L. Wang, Y. Wang, P. Prangnell, J. Robson, Modeling of Intermetallic Compounds Growth Between Dissimilar Metals, *Metall. Mater. Trans. A* 46(9) (2015) 4106-4114.

[71] F. Khodabakhshi, A.H. Kokabi, A. Simchi, Reactive friction-stir processing of nanocomposites: effects of thermal history on microstructure–mechanical property relationships, *Mater. Sci. Technol.* 33(15) (2017) 1776-1789.

Figure captions

Figure 1. (a, b) FE-SEM images from the titanium particles and (c) powder size distribution.

Figure 2. Stereographic macro-images from the thickness cross-section of cold sprayed and friction-stir modified titanium-coating layer on the aluminum alloy substrate.

Figure 3. The combined FE-SEM macro-image showing the selected regions for FIB sample extraction from the coating interface with aluminum substrate after cold spray and FSP steps.

Figure 4. FE-SEM images from the Al/Ti interface after (a-c) cold spray deposition and (d-f) friction-stir modification.

Figure 5. FIB sample preparation from the Al/Ti interface of FSP modified coating.

Figure 6. Bright-field TEM images from the Al/Ti interface after cold spray impact and FSP.

Figure 7. EDS elemental mapping analysis results from the prepared Al/Ti interface.

Figure 8. Grain structure of Ti-coating upon impact of cold spray deposition and thermo-mechanical action of FSP process.

Figure 9. TEM image showing the interface between aluminum substrate and titanium coating layer for more detailed studies.

Figure 10. Reaction layer under JEOL TEM contrast imaging at high magnification.

Figure 11. Titan LB TEM images showing the reaction layer between aluminum substrate and titanium coating layer.

Figure 12. HR-TEM images from the Al/Ti interface showing the wavy flow paths induced by severe plastic action of FSP process.

Figure 13. Atomic orientation at the interaction zone between aluminum and titanium at the interface.

Figure 14. Crystal structure analysis by FFT analysis from the interface.

Figure 15. EELS elemental mapping analysis results from the Al/Ti interface.

Figure 16. (a) The SEM image from Al-Ti interface showing the indexing points for Auger analysis. (b) Auger electron spectroscopy line-scan analysis results from the interaction zone at the interface. (c) The Boltzmann-Matano prediction results of inter-diffusion coefficient for aluminum though titanium.

Figure 17. Indentation hardness maps for the FSP modified cold sprayed sample from the (a) base metal toward the (b) Al/Ti interface and (c) coating layer.

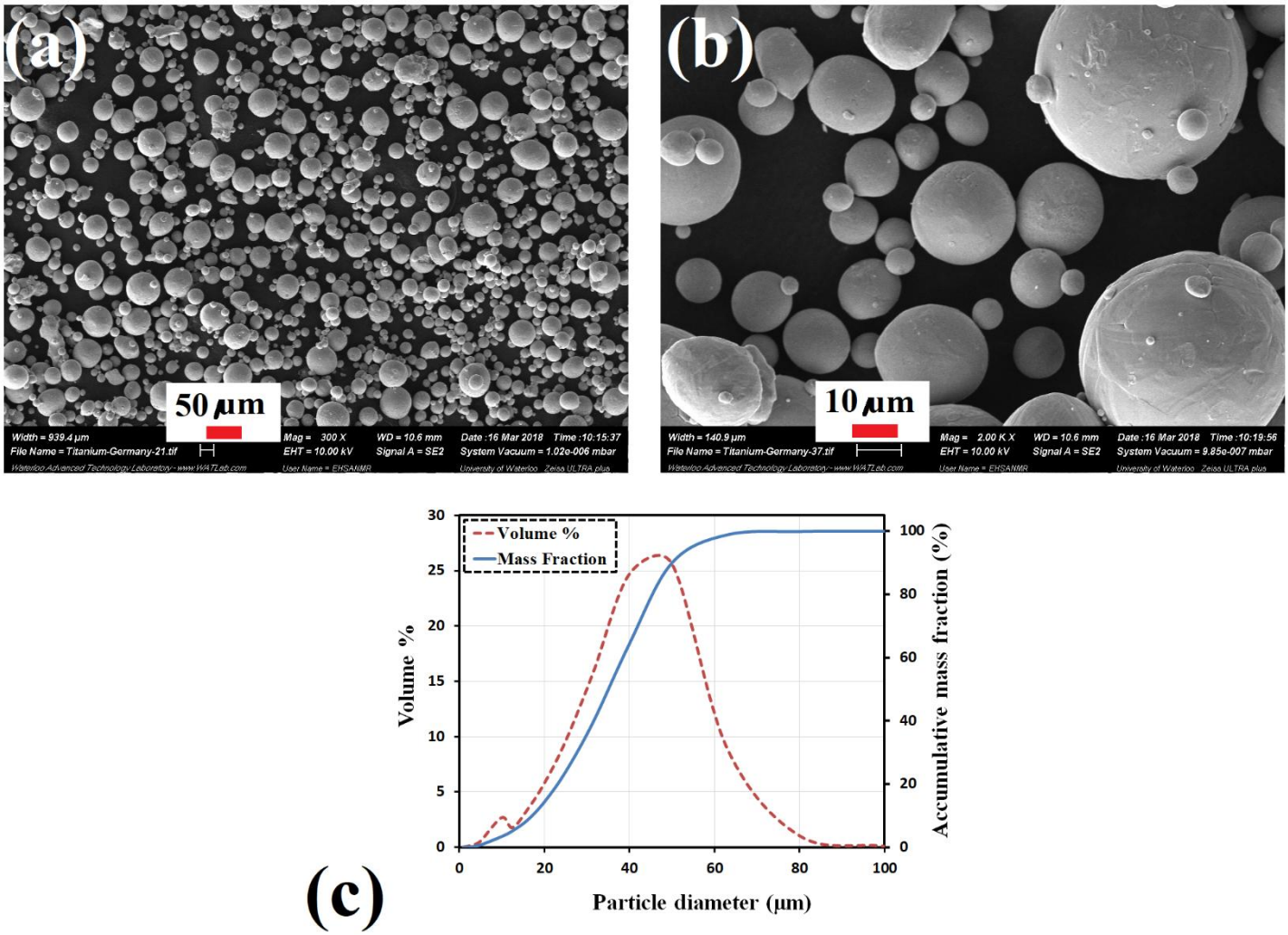
(a)
50 µm
Width = 939.4 µm
File Name = Titanium-Germany-21.tif
Mag = 300 X
EHT = 10.00 kV
WD = 10.6 mm
Signal A = SE2
Date :16 Mar 2018 Time :10:15:37
System Vacuum = 1.02e-006 mbar
(b)
10 µm
Width = 140.9 µm
File Name = Titanium-Germany-37.tif
Mag = 2.00 K X
EHT = 10.00 kV
WD = 10.6 mm
Signal A = SE2
Date :16 Mar 2018 Time :10:19:56
System Vacuum = 9.85e-007 mbar
(c)
Volume %
Mass Fraction
Volume %
Accumulative mass fraction (%)
Particle diameter (µm)
0
5
10
15
20
25
30
0
20
40
60
80
100

Figure 1

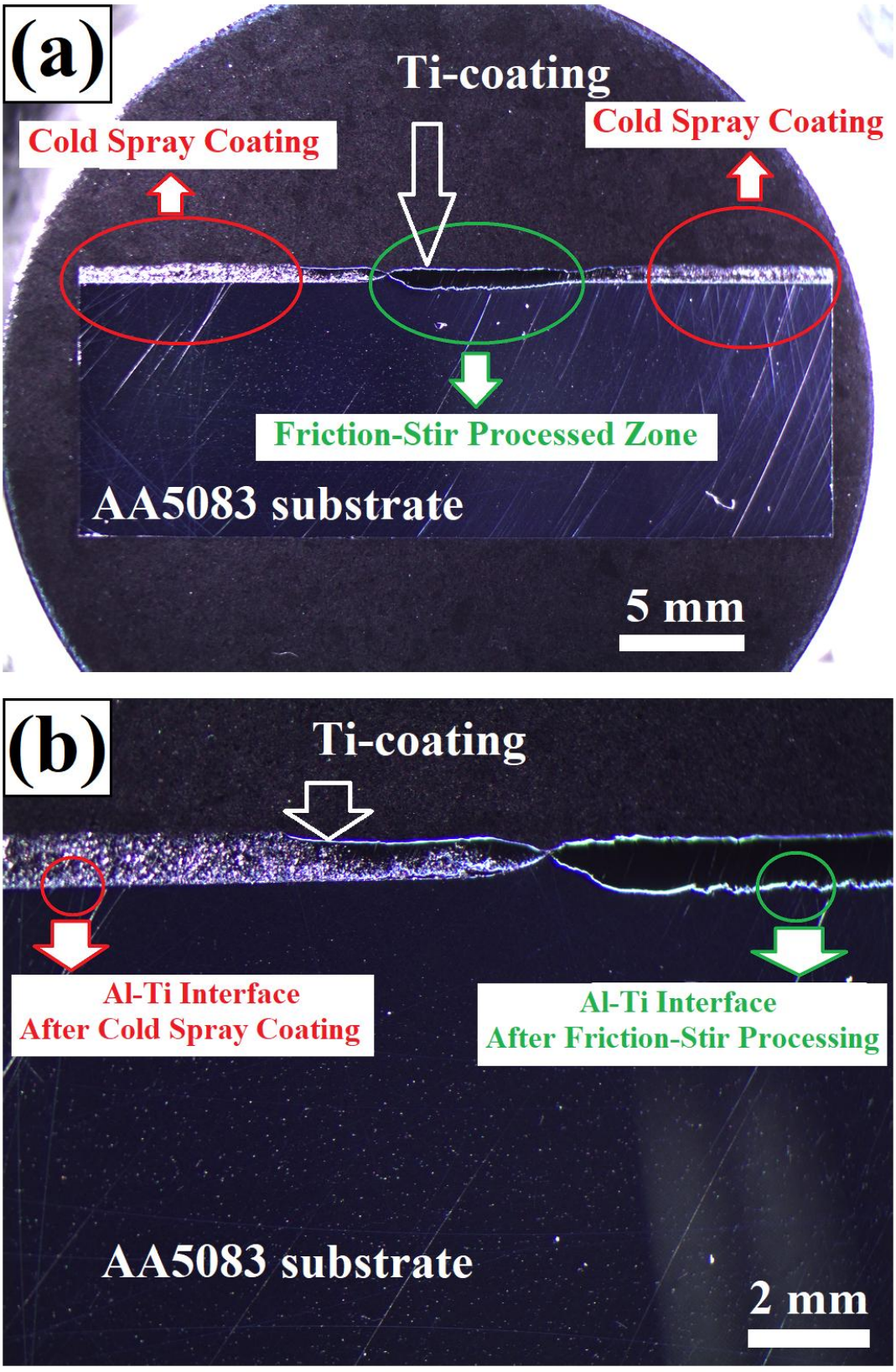
(a)
Ti-coating
Cold Spray Coating
Cold Spray Coating
Friction-Stir Processed Zone
AA5083 substrate
5 mm
(b)
Ti-coating
Al-Ti Interface
After Cold Spray Coating
Al-Ti Interface
After Friction-Stir Processing
AA5083 substrate
2 mm

Figure 2

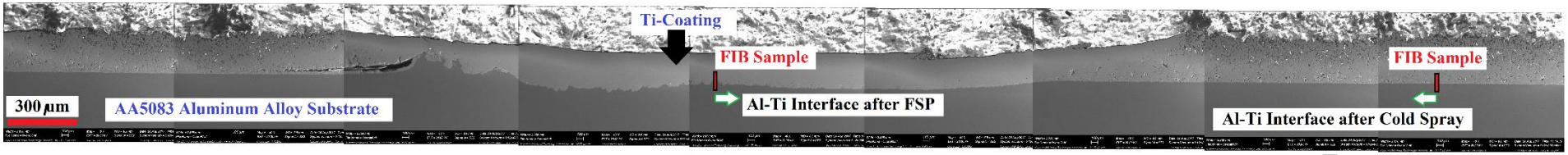

Figure 3

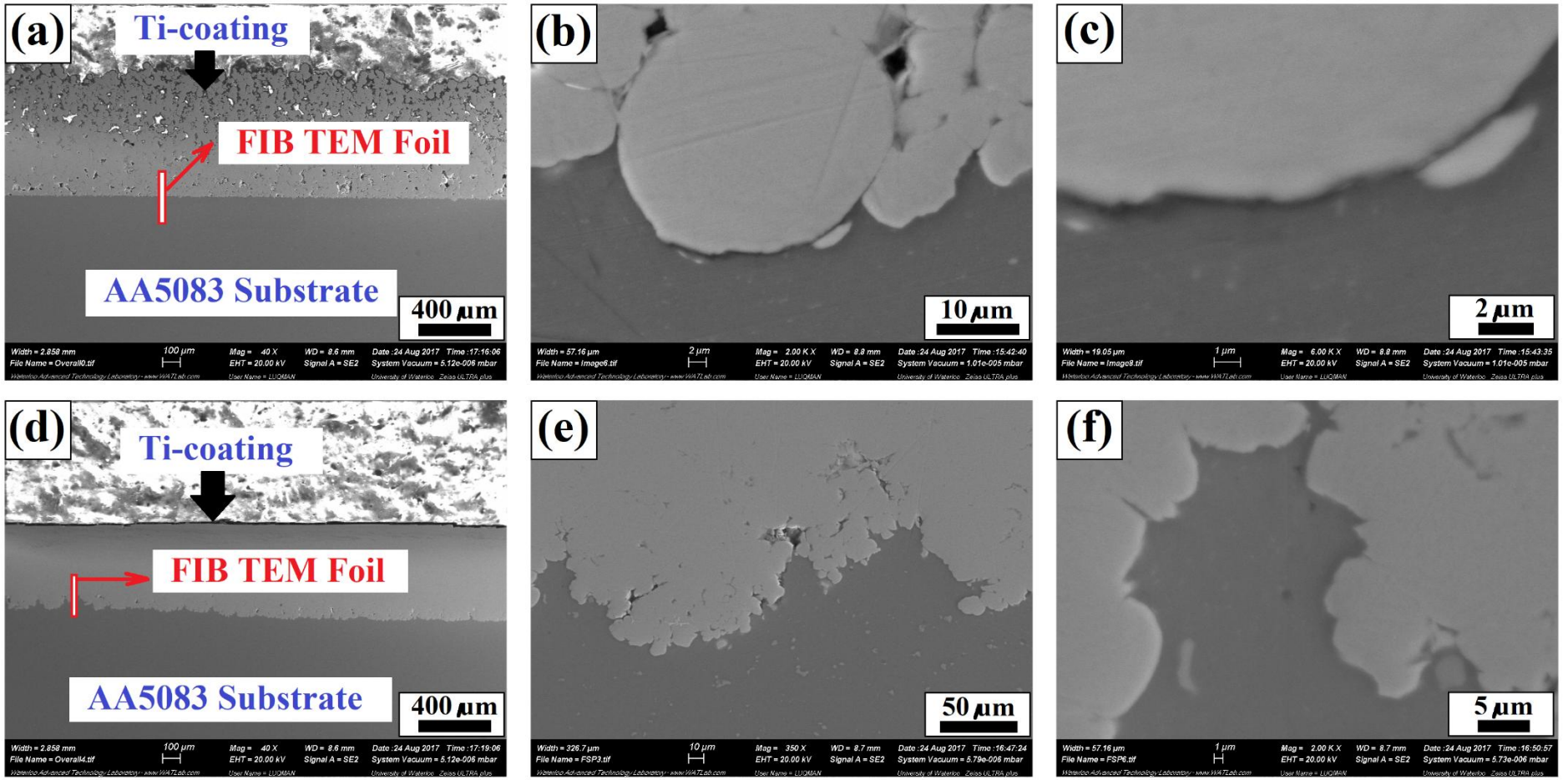

Figure 4

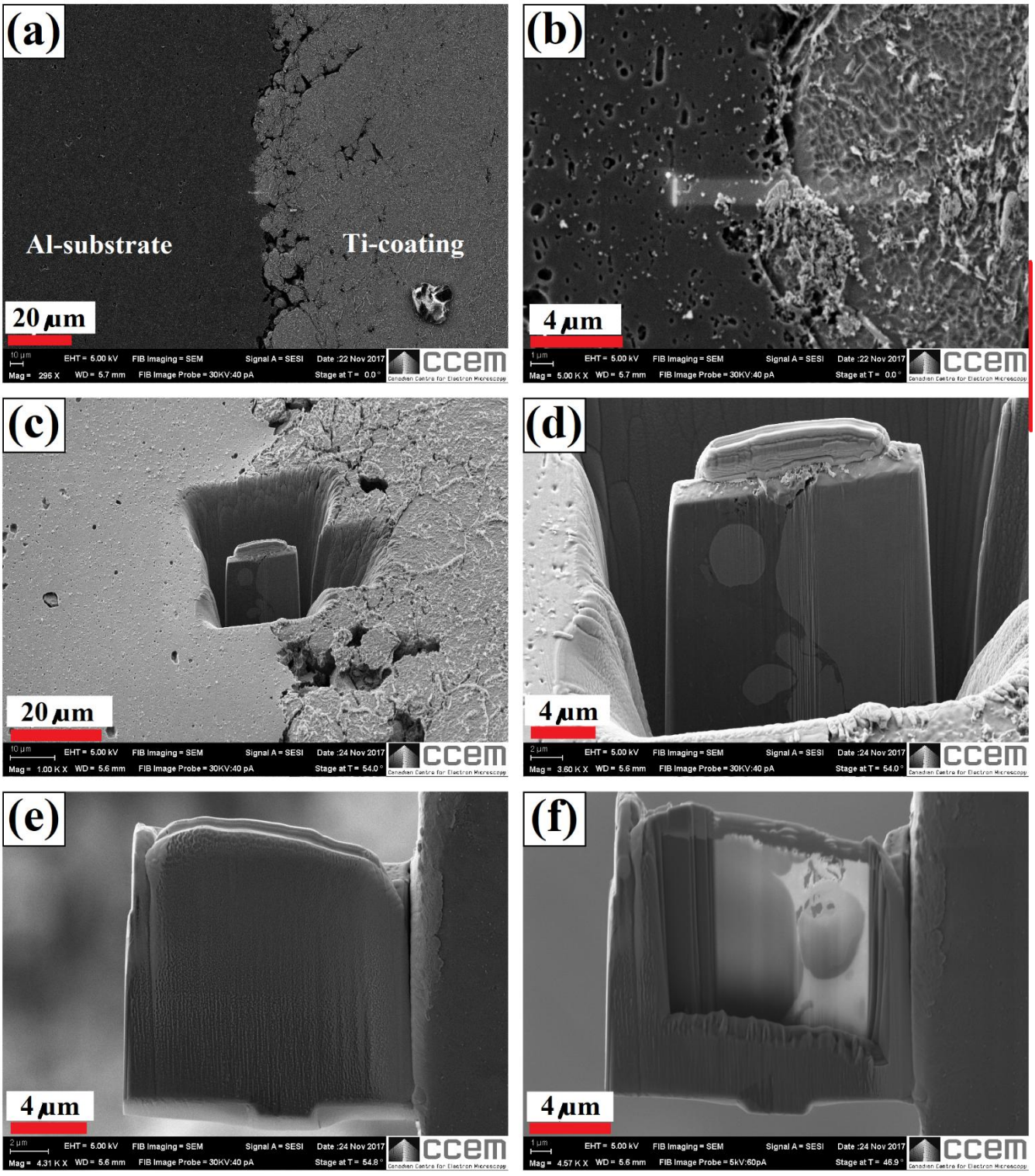

Figure 5

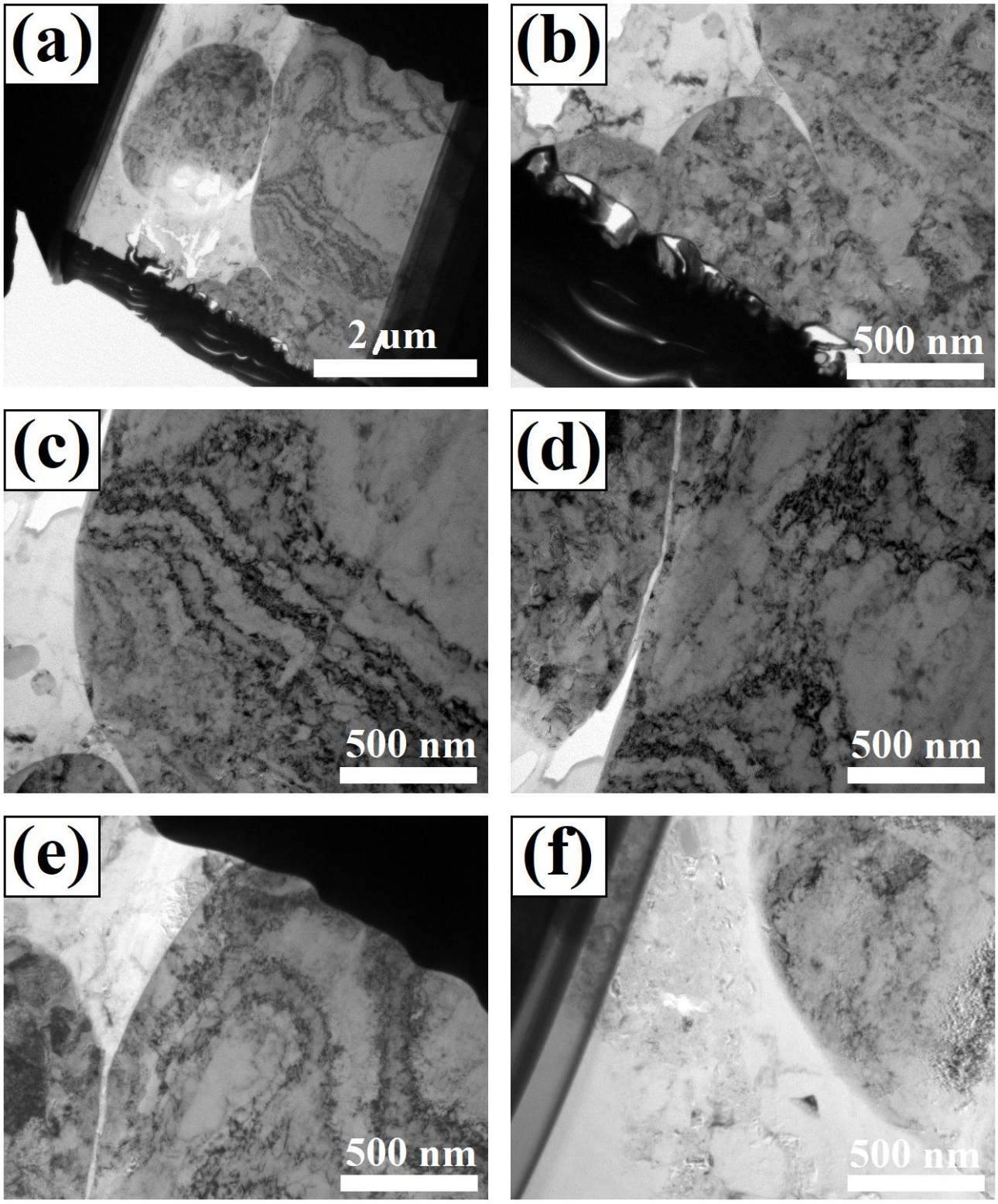

Figure 6

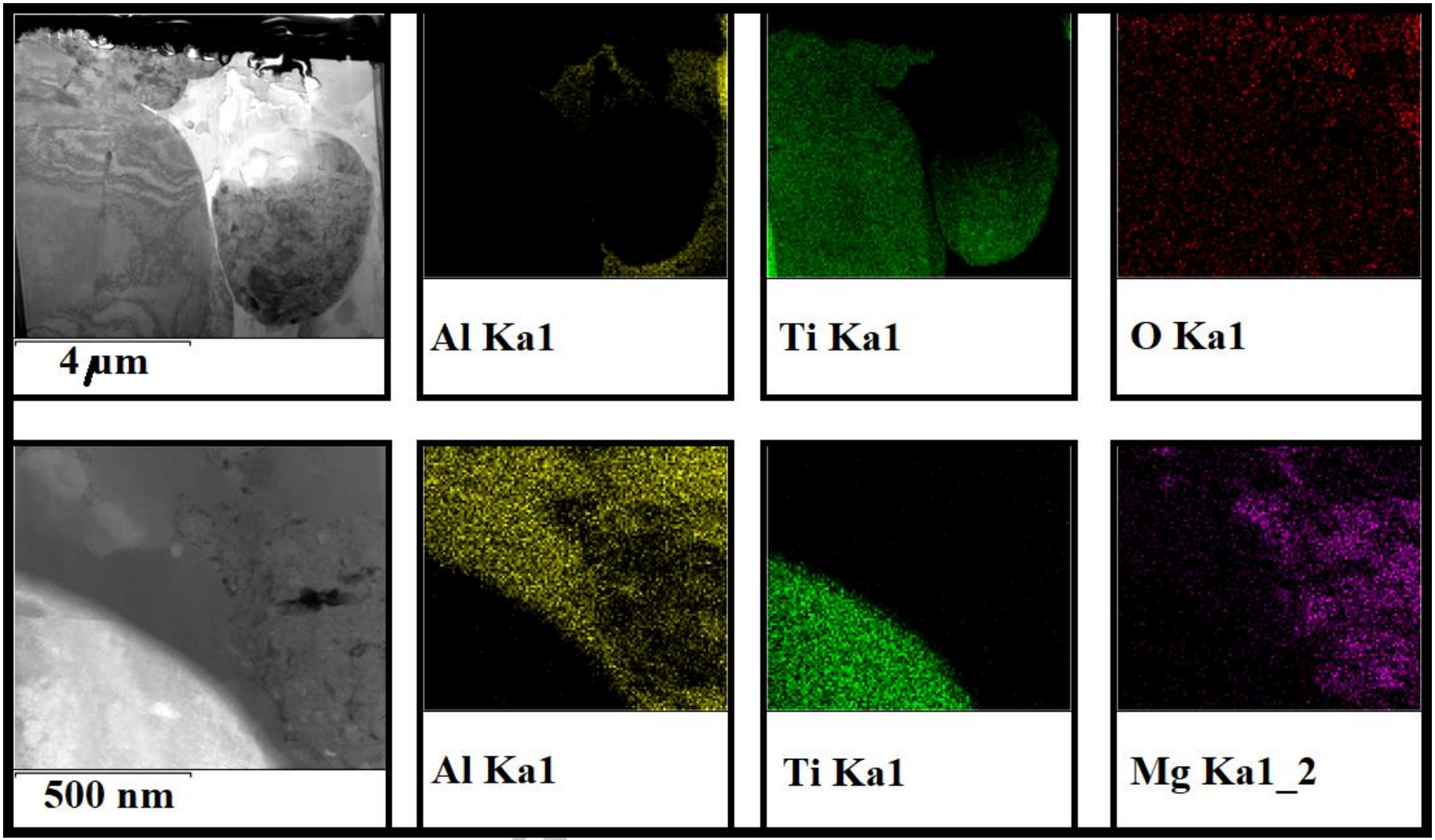

Figure 7

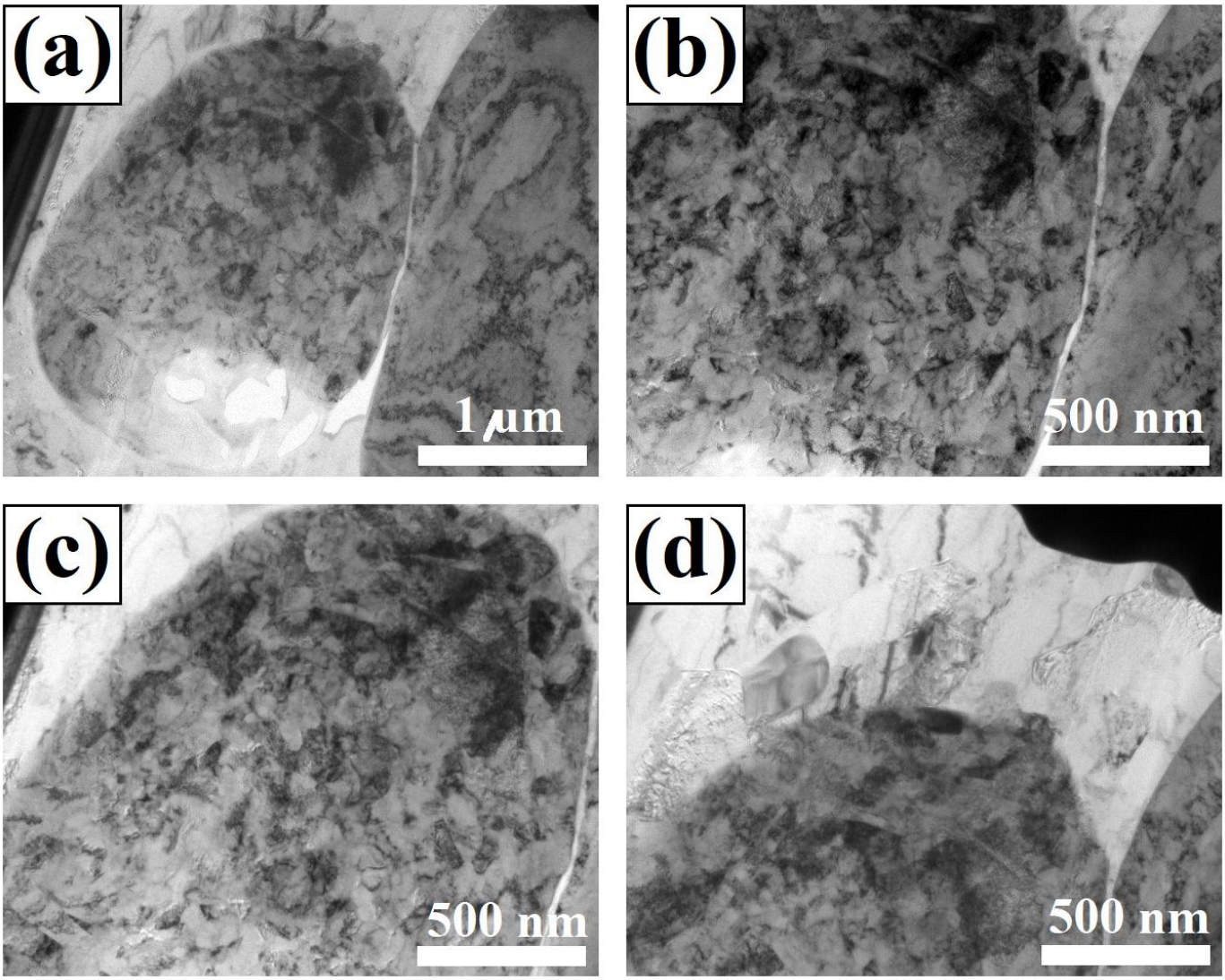

Figure 8

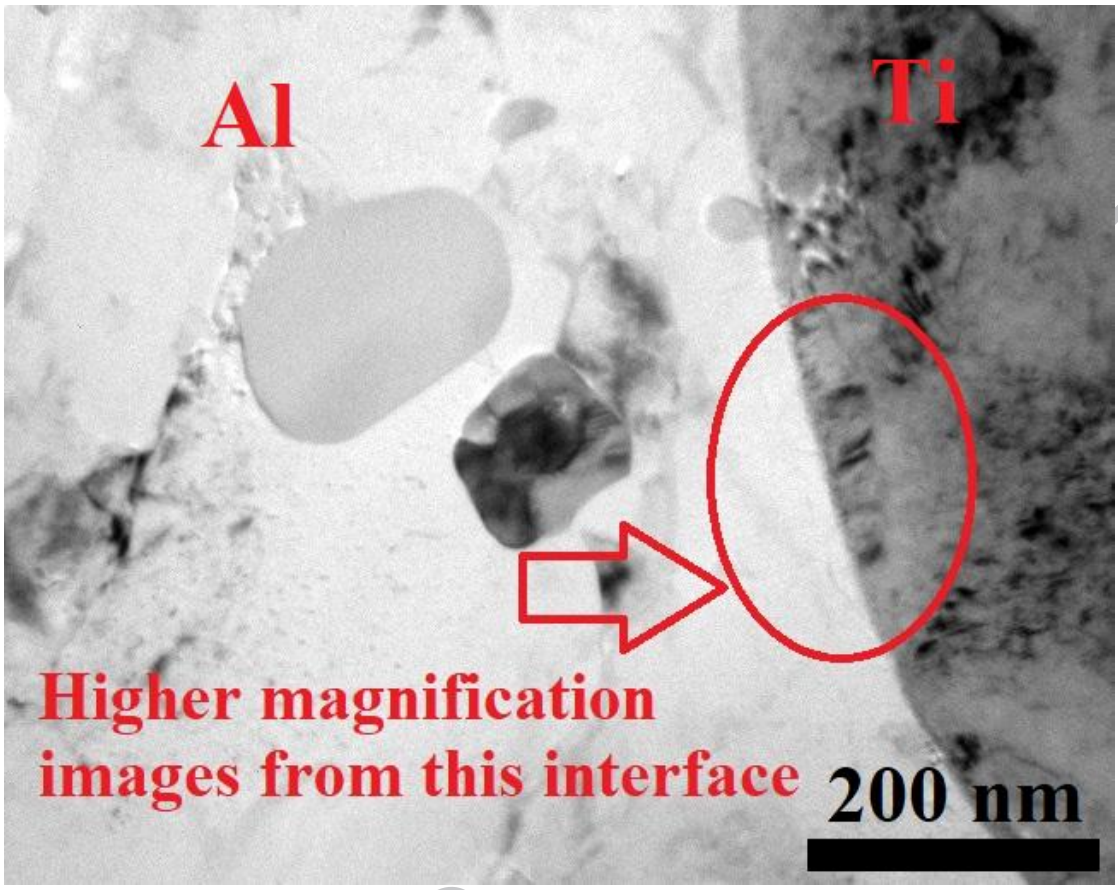

Figure 9

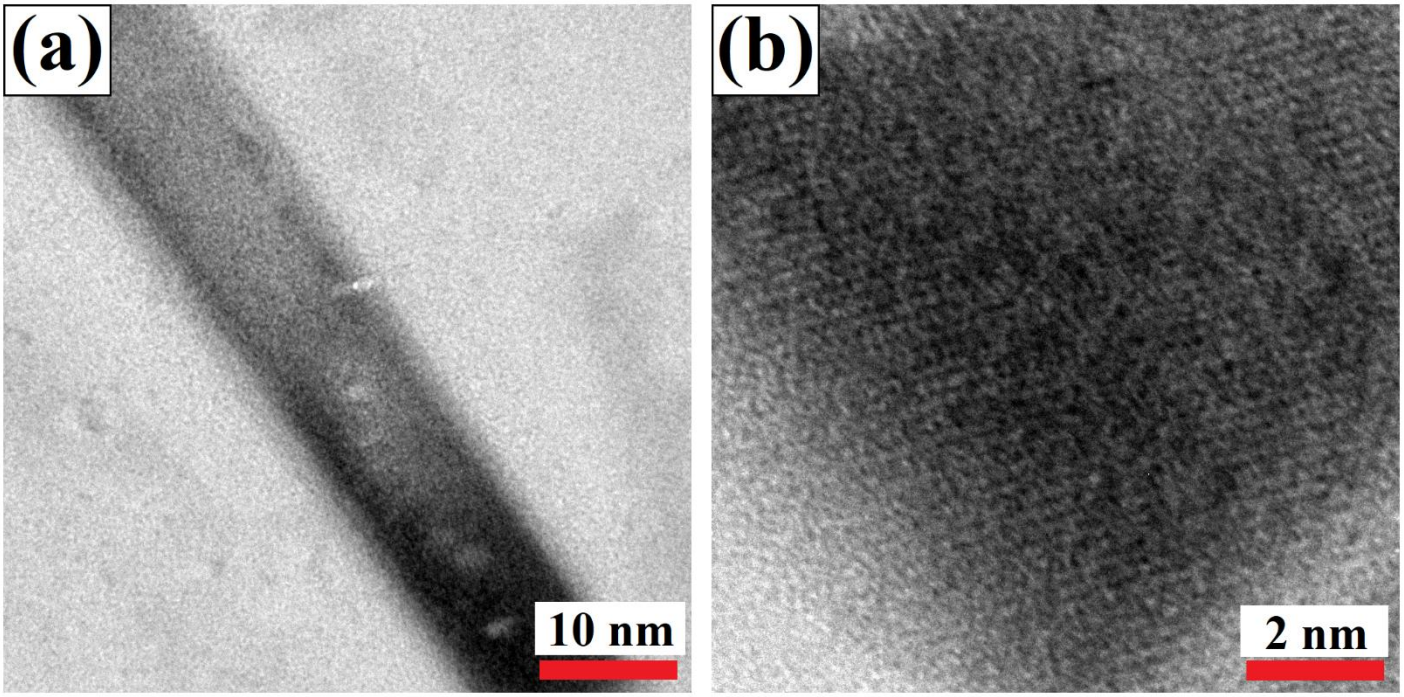

Figure 10

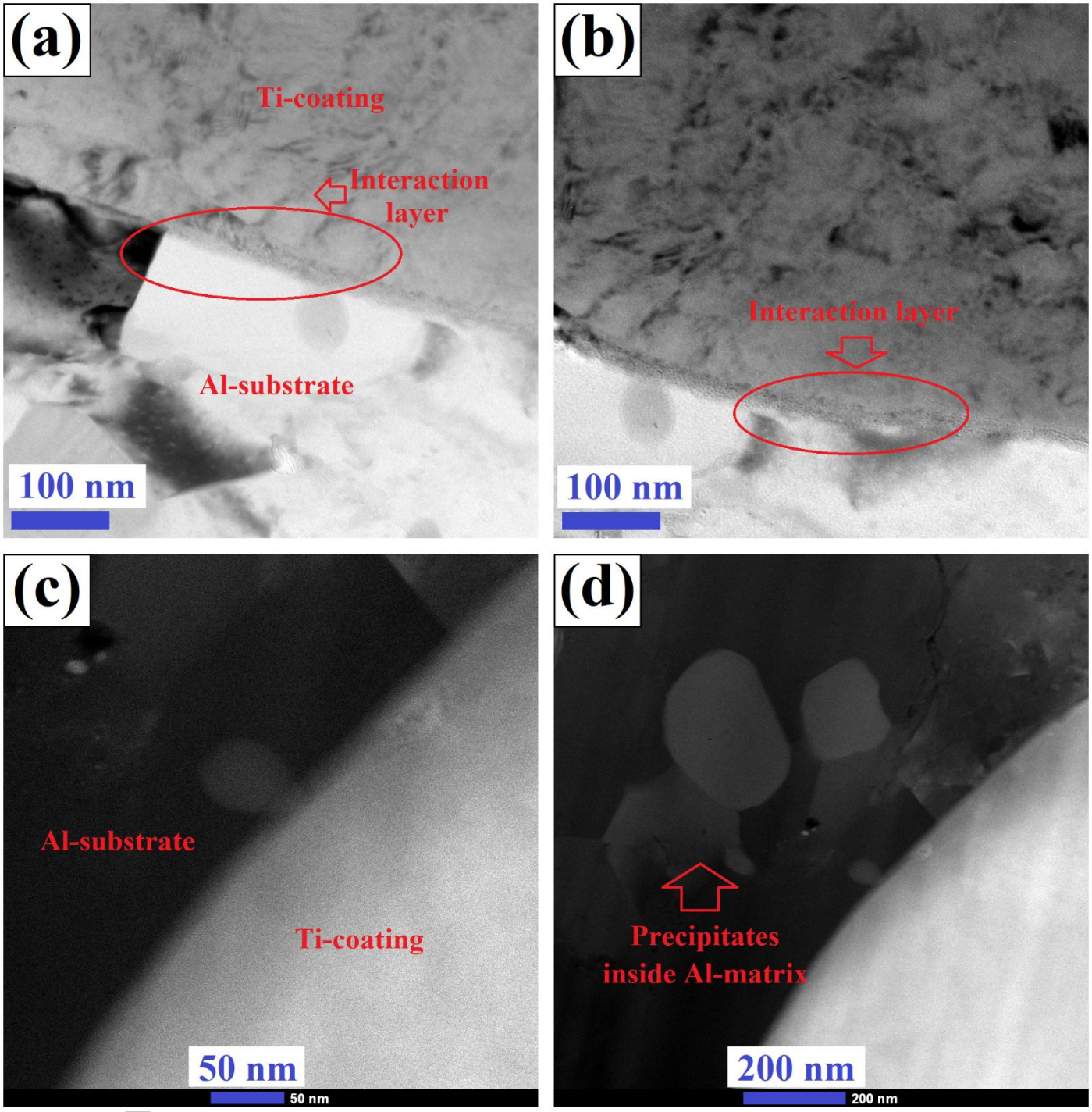
(a)
Ti-coating
Interaction layer
Al-substrate
100 nm
(b)
Interaction layer
100 nm
(c)
Al-substrate
Ti-coating
50 nm
50 nm
(d)
Precipitates inside Al-matrix
200 nm
200 nm

Figure 11

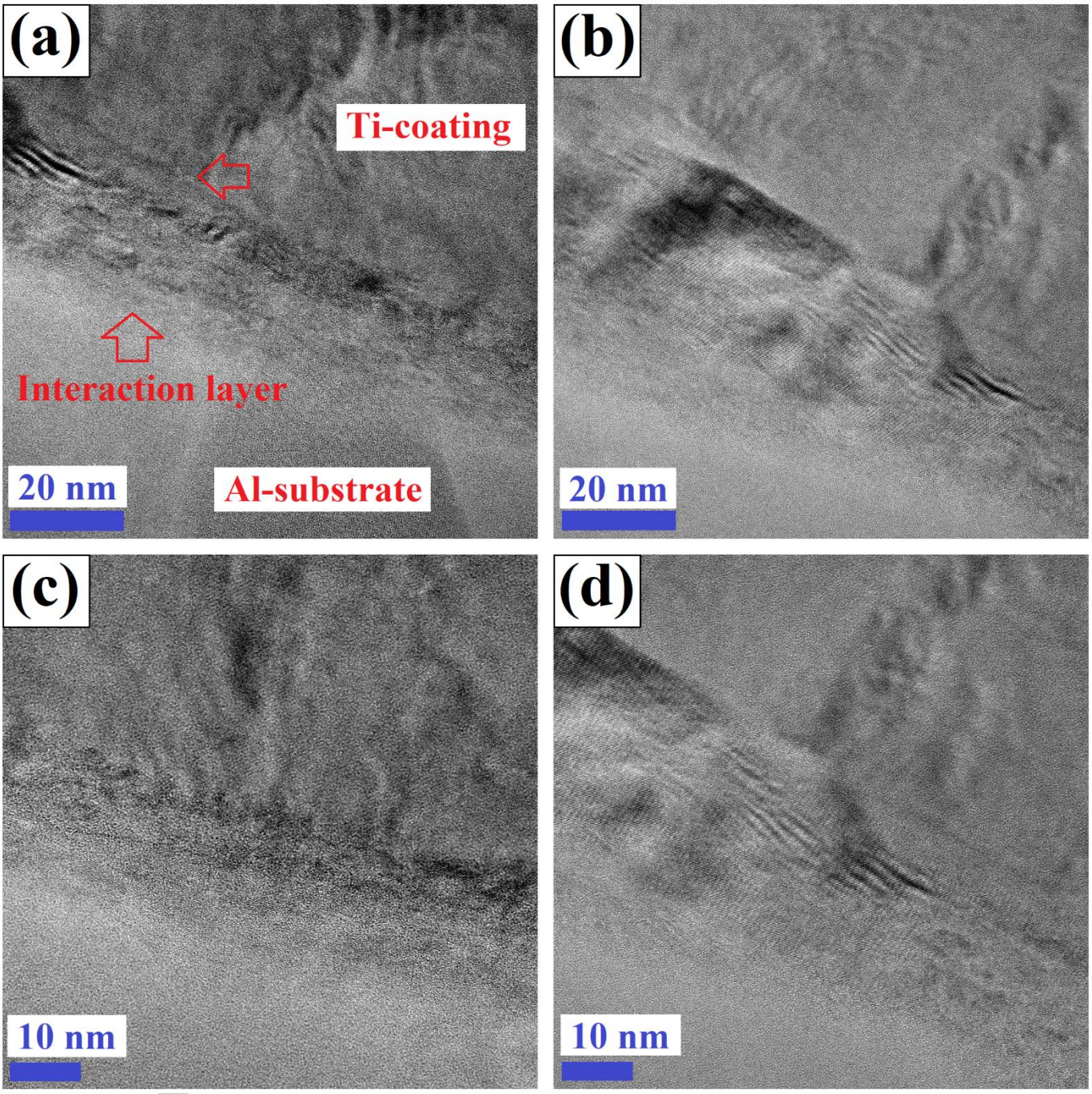
(a)
Ti-coating
Interaction layer
20 nm
Al-substrate
(b)
20 nm
(c)
10 nm
(d)
10 nm

Figure 12

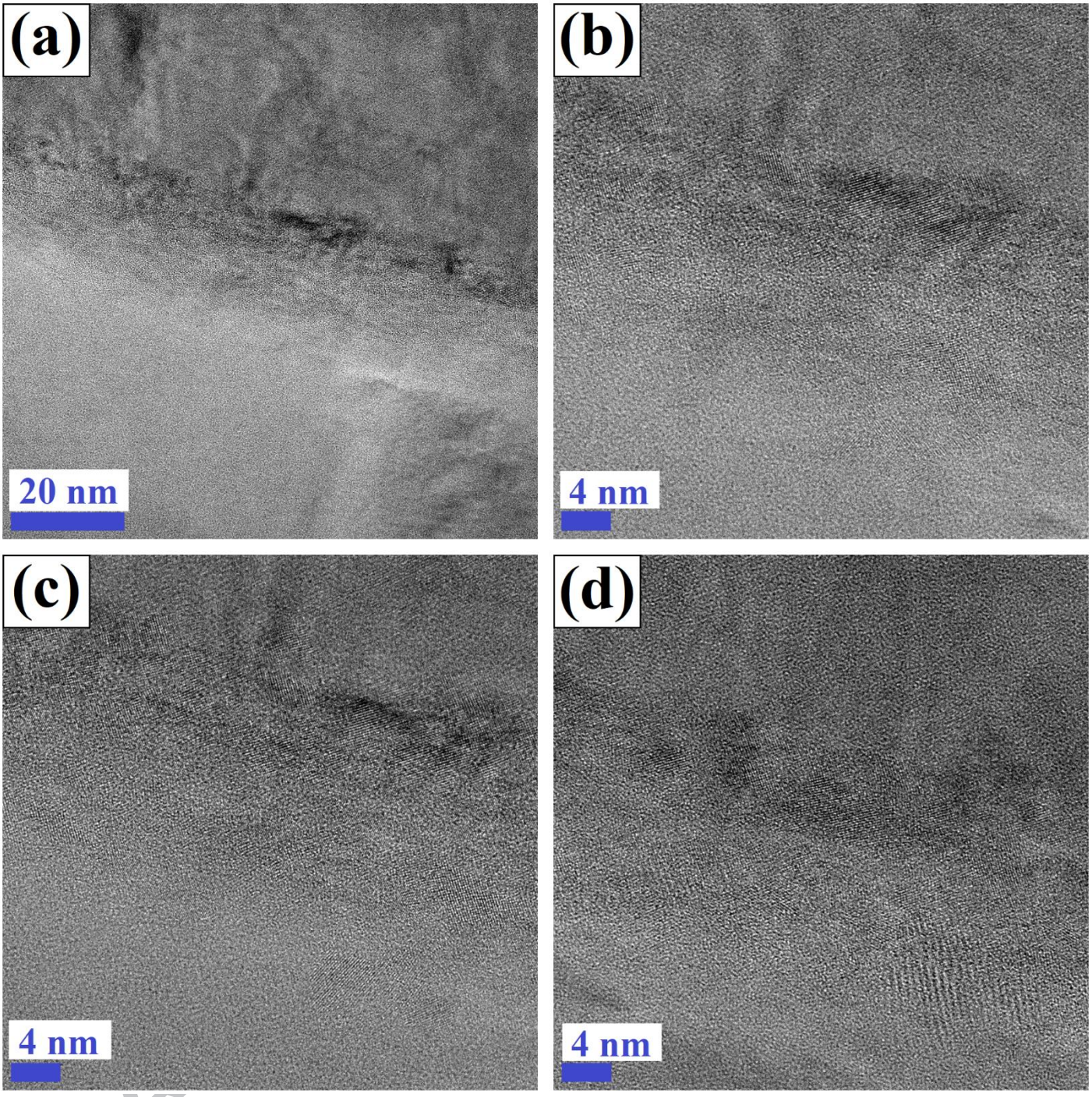

Figure 13

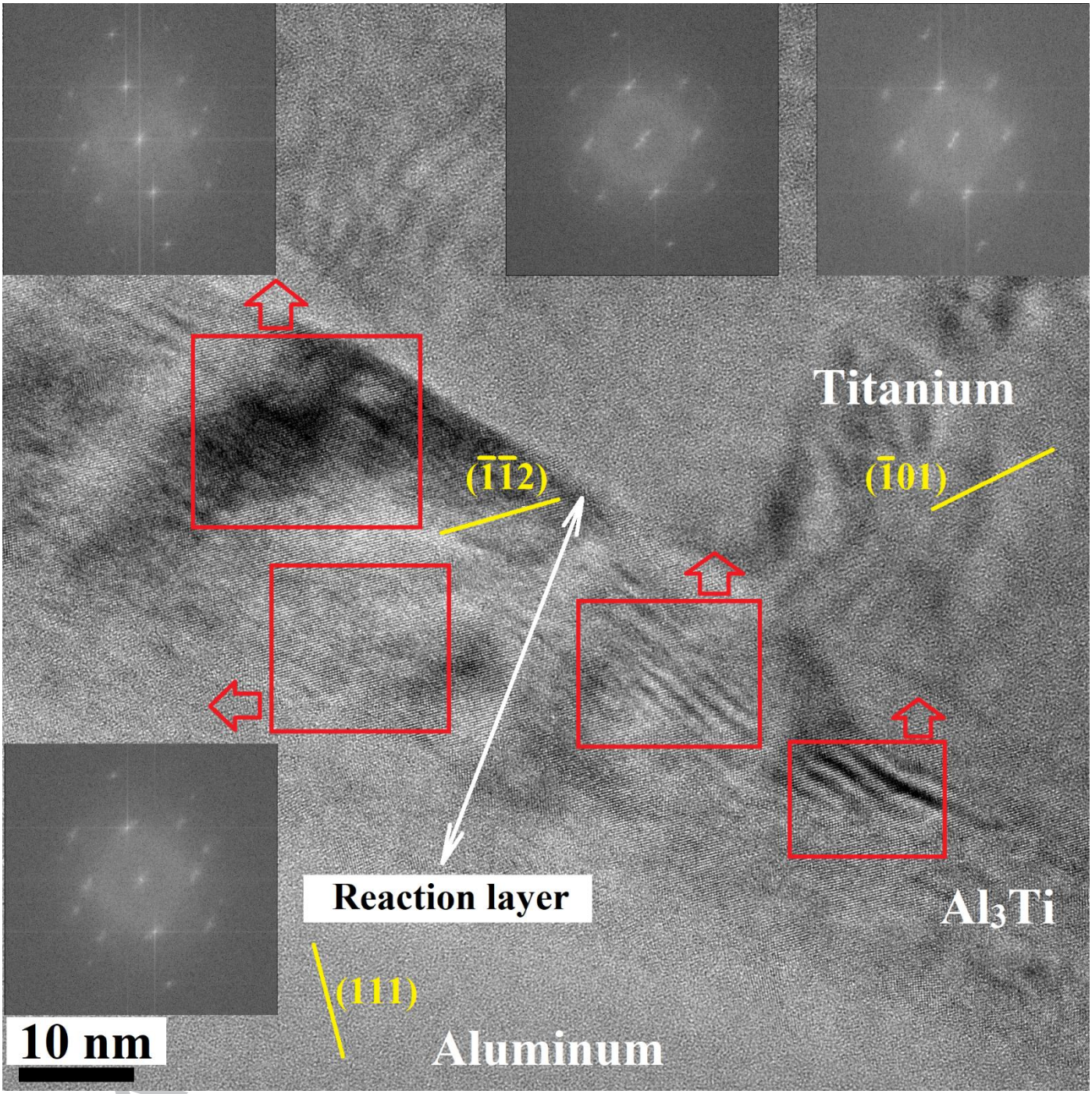
Titanium
$(\bar{1}\bar{1}2)$
$(\bar{1}01)$
Reaction layer
Al_3Ti
(111)
Aluminum
10 nm

Figure 14

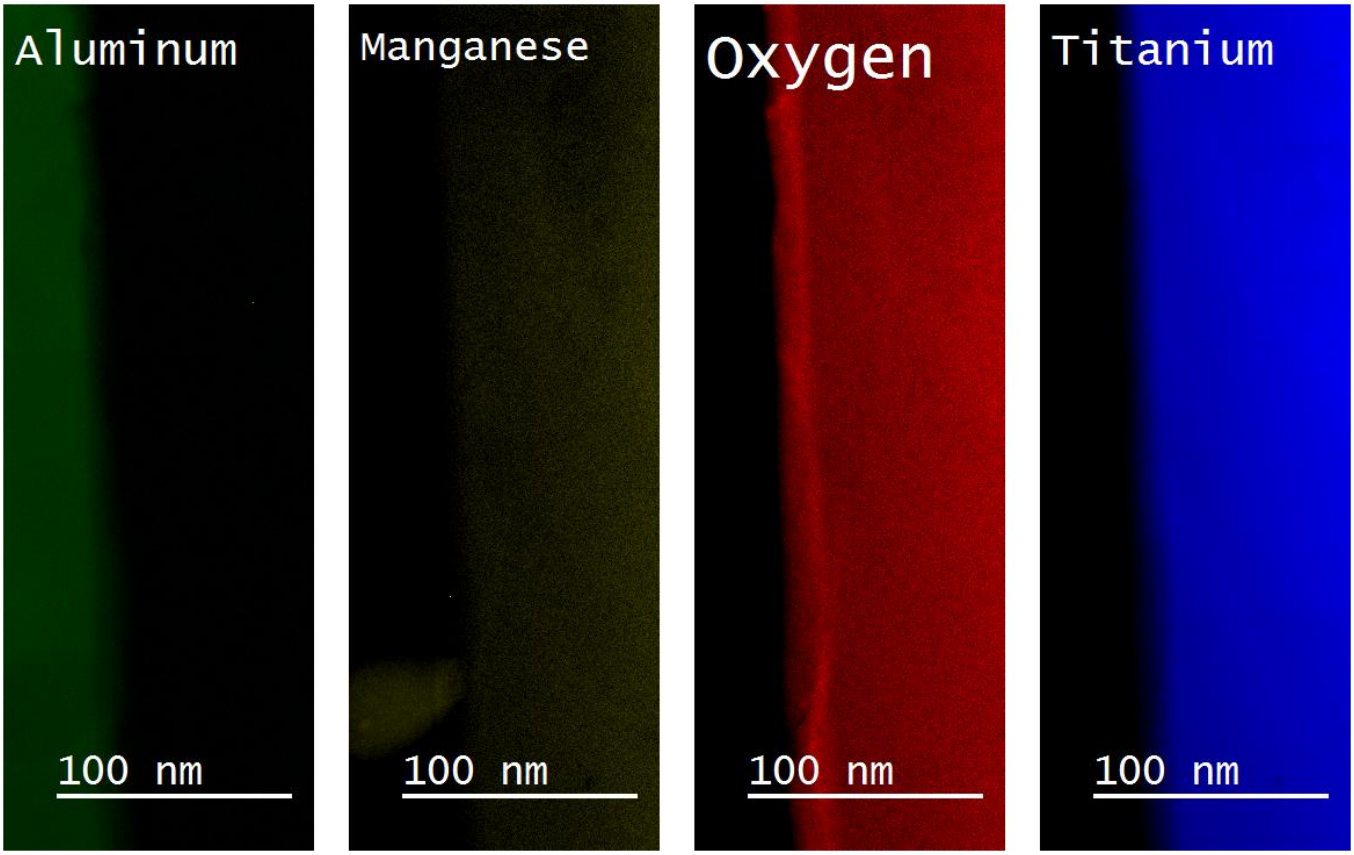

Figure 15

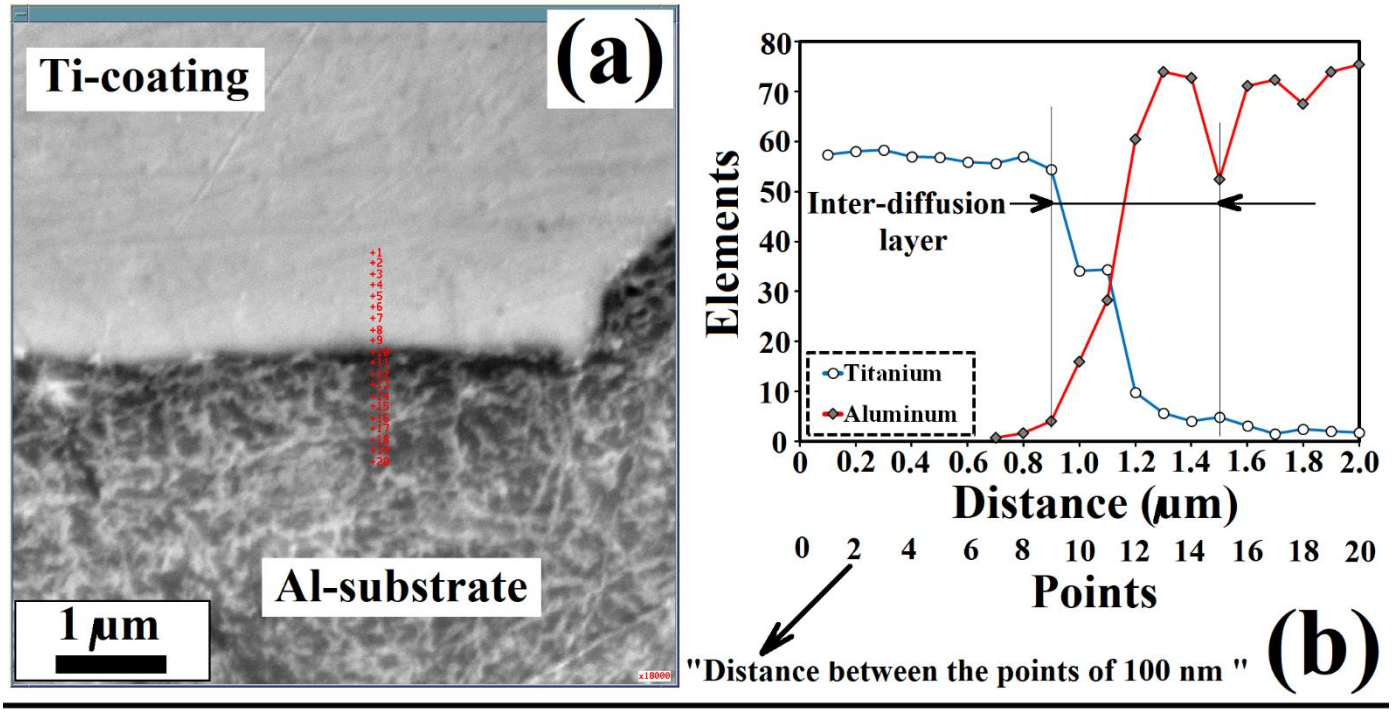
Ti-coating
(a)
Al-substrate
1 μm
Elements
Inter-diffusion layer
Titanium
Aluminum
Distance (μm)
Points
"Distance between the points of 100 nm "
(b)

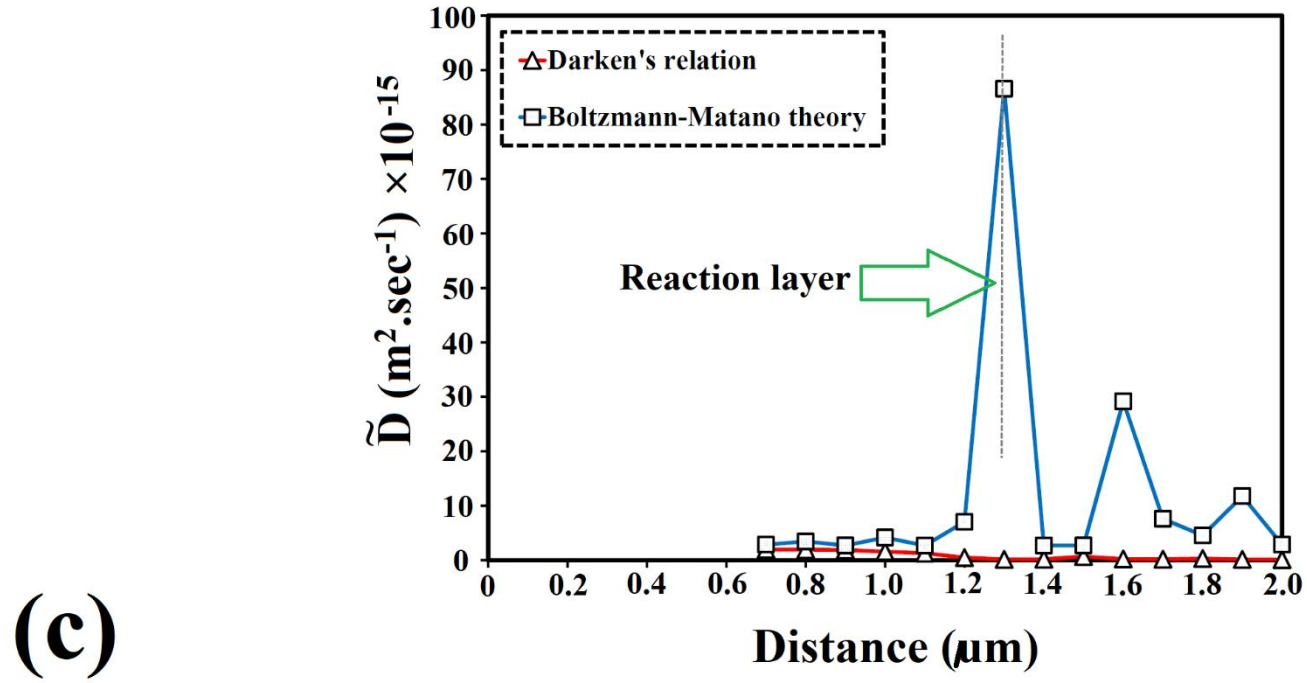
Darken's relation
Boltzmann-Matano theory
Reaction layer
$\tilde{D}$ (m^2.sec^{-1}) ×10^{-15}
Distance (μm)
(c)

Figure 16

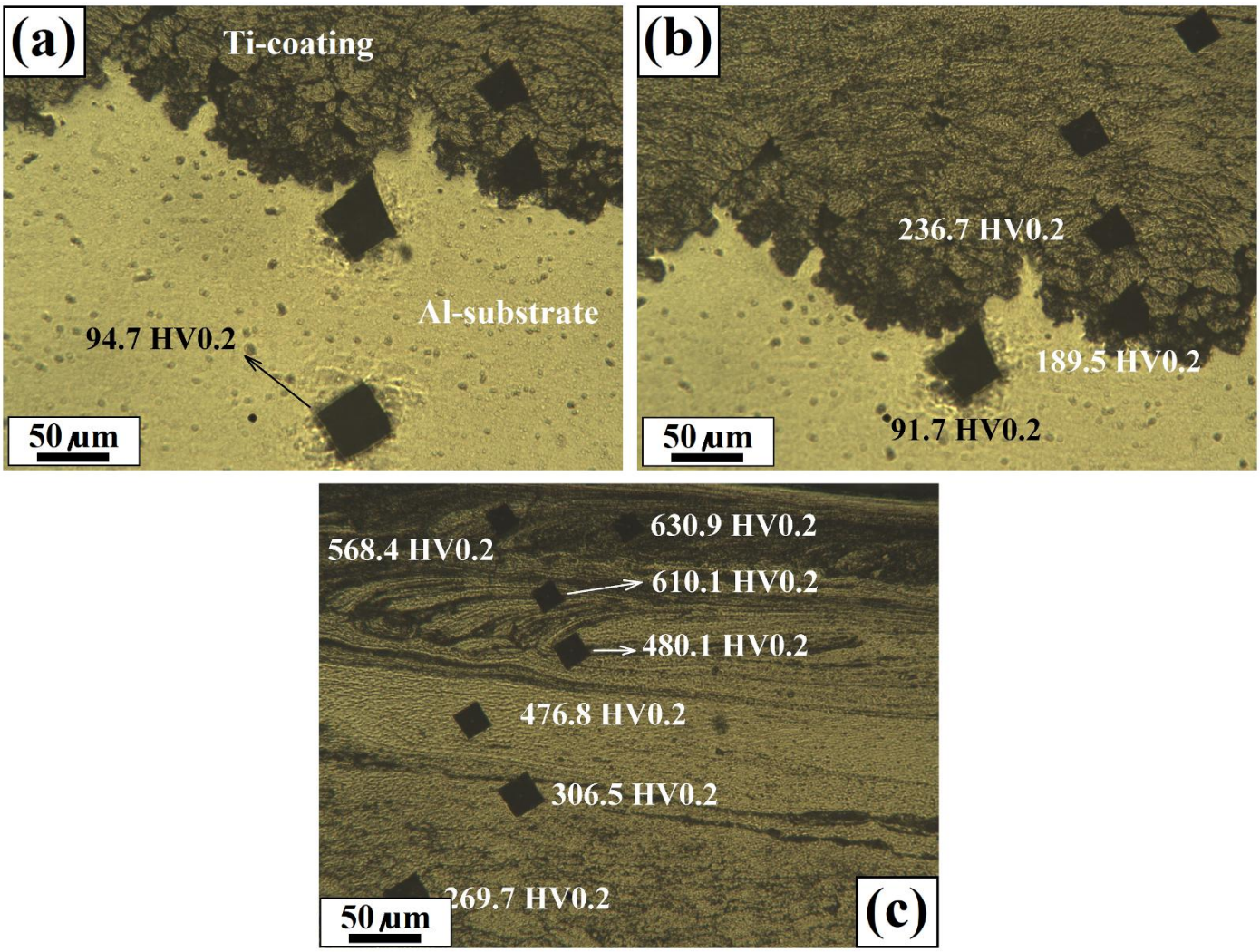

Figure 17

Table 1. Chemical composition for the studied AA5083 aluminum alloy as substrate (*wt*%).

Element	Al	Mg	Zn	Mn	Fe	Si	Ti
AA5083 alloy	Base	4.5	0.7	0.85	0.11	0.08	0.015

Research highlights:

- Friction-stir processing was employed to modify the structure of porous Ti-coating layer on the surface of an AA5083 alloy.
- Interaction layer between Al and Ti during cold spray coating and subsequent FSP step was studied.
- FIB-STEM analysis revealed the formation of a titanium-aluminide layer with average size of 10-20 nm at the interface.
- Diffusion modeling based on the auger spectroscopy analysis input predicted the same results.
- Chemical bonding was reported as the dominant mechanism during cold spraying deposition.

Graphical abstract